

# Molecular Tweezers Inhibit Islet Amyloid Polypeptide Assembly and Toxicity by a New Mechanism

Dahabada H. J. Lopes,<sup>†</sup> Aida Attar,<sup>†,‡</sup> Gayatri Nair,<sup>†</sup> Eric Y. Hayden,<sup>†</sup> Zhenming Du,<sup>||</sup> Kirsten McDaniel,<sup>†</sup> Som Dutt,<sup>⊥</sup> Heinz Bandmann,<sup>⊥</sup> Kenny Bravo-Rodriguez,<sup>#</sup> Sumit Mittal,<sup>#</sup> Frank-Gerrit Klärner,<sup>⊥</sup> Chunyu Wang,<sup>||</sup> Elsa Sanchez-Garcia,<sup>#</sup> Thomas Schrader,<sup>⊥</sup> and Gal Bitan<sup>\*,†,‡,§</sup>

<sup>†</sup>Department of Neurology, David Geffen School of Medicine, <sup>‡</sup>Brain Research Institute, and <sup>§</sup>Molecular Biology Institute, University of California at Los Angeles, Los Angeles, California 90095-7334, United States

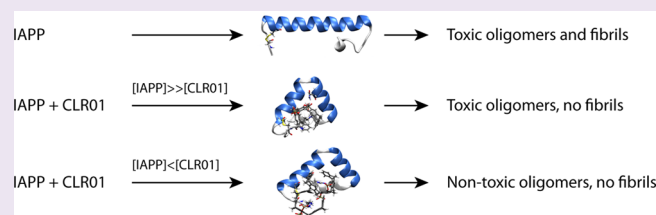
<sup>||</sup>Department of Biology, Rensselaer Polytechnic Institute, Troy, New York 12180, United States

<sup>⊥</sup>Institute of Organic Chemistry, University of Duisburg-Essen, 45141 Essen, Germany

<sup>#</sup>Max-Planck-Institut für Kohlenforschung, 45470 Mülheim an der Ruhr, Germany

## Supporting Information

**ABSTRACT:** In type-2 diabetes (T2D), islet amyloid polypeptide (IAPP) self-associates into toxic assemblies causing islet  $\beta$ -cell death. Therefore, preventing IAPP toxicity is a promising therapeutic strategy for T2D. The molecular tweezer CLR01 is a supramolecular tool for selective complexation of K residues in (poly)peptides. Surprisingly, it inhibits IAPP aggregation at substoichiometric concentrations even though IAPP has only one K residue at position 1, whereas efficient inhibition of IAPP toxicity requires excess CLR01. The basis for this peculiar behavior is not clear. Here, a combination of biochemical, biophysical, spectroscopic, and computational methods reveals a detailed mechanistic picture of the unique dual inhibition mechanism for CLR01. At low concentrations, CLR01 binds to K1, presumably nucleating nonamyloidogenic, yet toxic, structures, whereas excess CLR01 binds also to R11, leading to nontoxic structures. Encouragingly, the CLR01 concentrations needed for inhibition of IAPP toxicity are safe *in vivo*, supporting its development toward disease-modifying therapy for T2D.



Type-2 diabetes (T2D) is the most common amyloid-related disease affecting hundreds of millions of people worldwide.<sup>1</sup> It is an acquired syndrome closely associated with obesity and elevated blood glucose levels due to progressive insulin resistance and exhaustion of insulin-producing pancreatic islet  $\beta$ -cells. T2D sequelae include ocular, renal, cardiovascular, and neurologic complications,<sup>2</sup> increasing morbidity and mortality<sup>3</sup> and causing a substantial economic and public health burden.<sup>4</sup>

Islet amyloid polypeptide (IAPP), a 37-residue polypeptide hormone,<sup>5</sup> is the major component of the pancreatic islet amyloid associated with T2D and is one of the most amyloidogenic polypeptides known.<sup>6</sup> It is processed and stored with insulin in the secretory granules of  $\beta$ -cells and is secreted as a soluble monomer at low pM concentrations.<sup>7</sup> In T2D, IAPP self-assembles into toxic oligomers that cause damage to  $\beta$ -cell membranes and mitochondria, leading to apoptosis. Eventually, IAPP precipitates as extracellular pancreatic amyloid, a pathologic hallmark of T2D. The conversion from monomer to oligomers and then to amyloid is accompanied by a conformational transition from structures with substantial  $\alpha$ -helix content to  $\beta$ -sheet-rich fibrils.<sup>8–10</sup> The  $\beta$ -sheet-rich core region of IAPP fibrils initially was believed to comprise only residues 20–29.<sup>11</sup> However, multiple other regions, including

residues 8–20, 10–19, 13–18, 17–29, and 30–37, have been reported also to be involved in amyloid formation.<sup>12</sup> Solid-state NMR studies have shown that residues 8–17 and 28–37 form parallel, in-register  $\beta$ -sheets in IAPP fibrils.<sup>13</sup>

IAPP monomers and monomer dimerization also have been investigated theoretically.<sup>14–19</sup> Replica-Exchange Molecular Dynamics (REMD) simulations showed that, in solution, the peptide adopts a variety of conformations ranging from extended to kinked. Concomitant with these global conformational changes, the secondary structure also varies and comprises coil,  $\alpha$ -helix, and intramolecular  $\beta$ -sheet as the most common structural motifs.<sup>14–16</sup> REMD simulations of dimerization suggested that a defined secondary structure in the monomer favors dimer formation. In this context, Dupuis et al. have shown that free-energy changes associated with dimer formation increase in monomers with higher levels of  $\alpha$ -helix or  $\beta$ -strand motifs.<sup>17</sup> Using Hamiltonian and temperature (HT)-REMD simulations, Laghaei et al. found that the IAPP monomer might adopt a stable  $\alpha$ -helix structure spanning

Received: May 23, 2014

Accepted: April 6, 2015

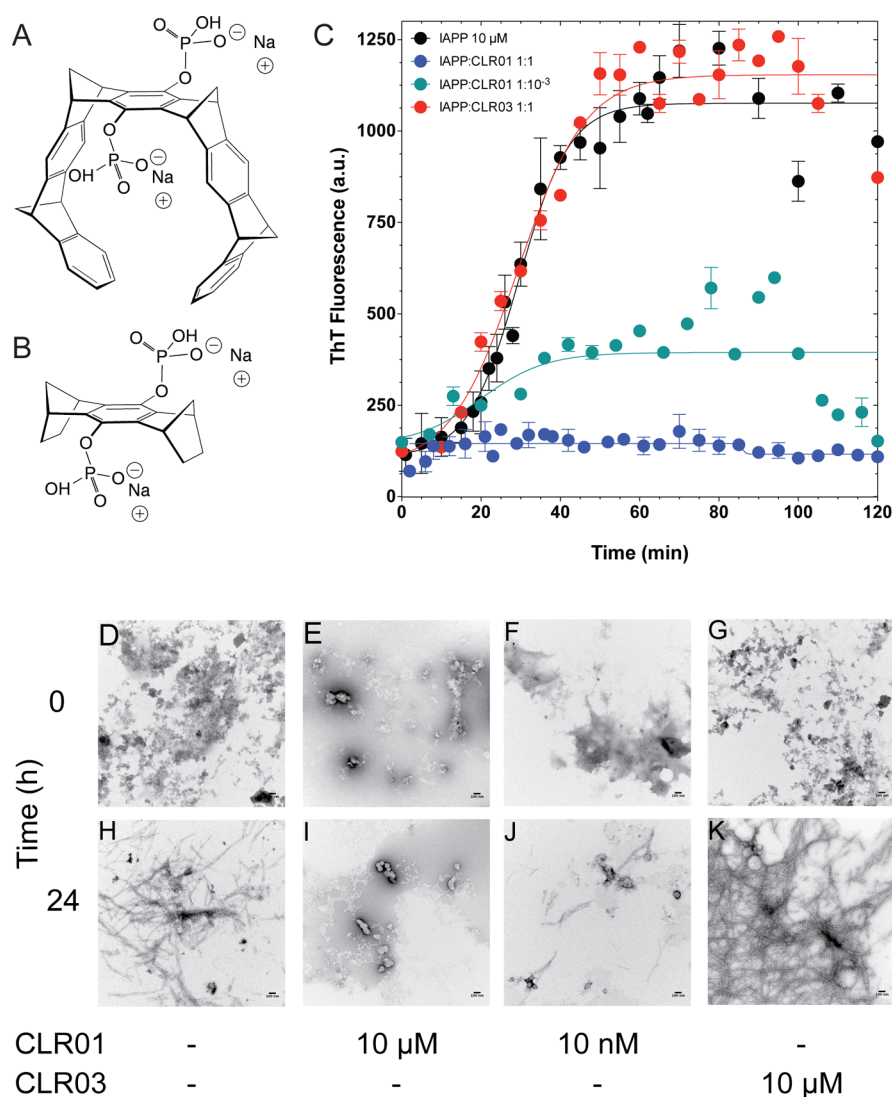


**Figure 1.** CLR01 inhibits IAPP  $\beta$ -sheet and fibril formation. (A) Schematic structure of CLR01. (B) Schematic structure of CLR03. The compounds are slightly basic in aqueous solution, and the phosphate groups are partially protonated at pH 7.4. (C) IAPP ( $10 \mu\text{M}$ ) was incubated in the absence or presence of CLR01 or CLR03 at  $25^\circ\text{C}$  with constant agitation, and formation of  $\beta$ -sheet was measured using the ThT fluorescence assay. The data are presented as mean  $\pm$  SEM of six independent experiments. (D–K) Aliquots were taken at  $t = 0$  or 24 h and examined by EM. The images are representative of three independent experiments. Scale bars denote 100 nm.

residues 5 to 16 and that in the dimer, this helix favors hydrophobic interactions of Leu12 with Phe15 and Leu16.<sup>18</sup>

To date, two main classes of inhibitors of IAPP amyloidogenicity and/or cytotoxicity have been described. The first group consists of small molecules, typically containing one or more aromatic rings, which suppress fibril formation.<sup>20–24</sup> Some of these compounds have been reported also to inhibit IAPP cytotoxicity and to prevent amyloidogenicity and/or cytotoxicity by other amyloidogenic proteins.<sup>23,25</sup> The second class includes synthetic, IAPP-derived peptides based on the concept of self-recognition. These peptides may be derivatives of full-length IAPP<sup>26,27</sup> or comprise IAPP segments.<sup>28,29</sup> Often these IAPP derivatives contain *N*-methylated amino acids and/or amino acid substitutions designed to decrease amyloidogenicity. Despite the progress made in these directions, to date, there is no disease-modifying therapy for T2D.

In search for novel means of modulating amyloid proteins self-association and inhibiting their toxicity, we identified

“molecular tweezers” (MTs) that operate by a novel mechanism.<sup>30</sup> These compounds are artificial receptors that bind selectively to K residues, typically with  $K_d \approx 10 \mu\text{M}$ , although submicromolar affinity can be achieved in certain cases.<sup>31</sup> MTs bind with 5–10 times lower affinity to R, and with little, if any affinity to most other cationic biomolecules.<sup>30,32–34</sup> IAPP has only one K residue at position 1, and therefore, we did not expect our lead MT, CLR01 (Figure 1A), to inhibit its assembly or toxicity. However, in initial experiments, we found that aggregation of  $10 \mu\text{M}$  IAPP was inhibited completely by  $1 \mu\text{M}$  CLR01.<sup>30</sup> Interestingly, in contrast to other amyloidogenic proteins, for which inhibition of aggregation and inhibition of toxicity were observed at similar protein/CLR01 concentration ratios, inhibition of IAPP-induced toxicity required excess CLR01. This intriguing behavior suggested that binding of CLR01 to IAPP might lead to different structural consequences than with other amyloidogenic proteins. To explore further this unexpected behavior and evaluate the therapeutic potential of CLR01 for T2D, we employed a combination of biochemical,

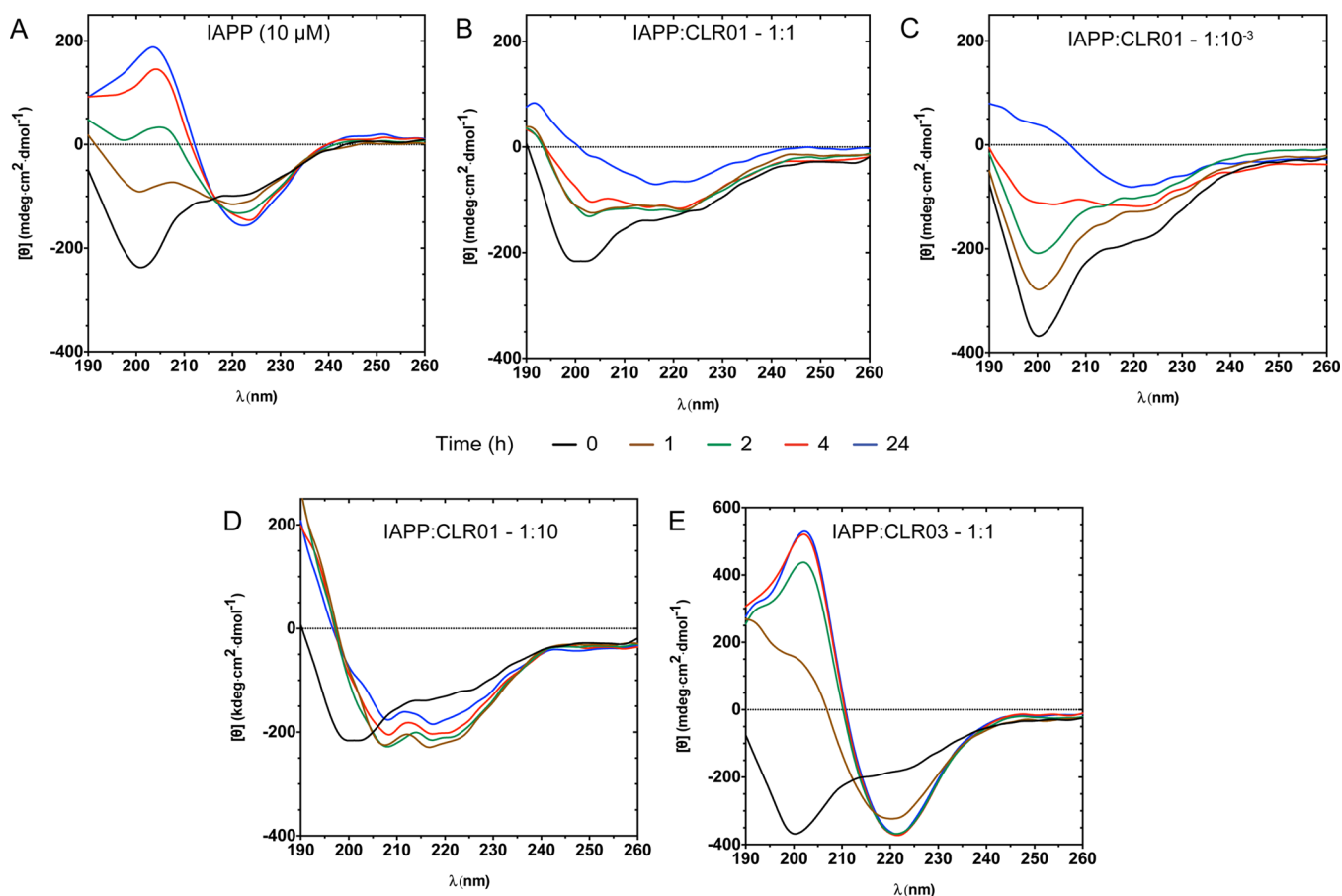


**Figure 2.** CLR01 induces time-dependent conformational changes in IAPP. IAPP ( $10 \mu\text{M}$ ) was incubated in the absence or presence of CLR01 or CLR03 at  $25^\circ\text{C}$  with constant agitation in 1 mm path length quartz cuvettes, and CD spectra were recorded at the indicated time points. The spectra are representative of four independent experiments.

biophysical, and computational methods to elucidate the mechanism by which CLR01 binds to IAPP and inhibits its assembly and toxicity.

## RESULTS AND DISCUSSION

**CLR01 Inhibits IAPP Amyloid Formation *In Vitro* at Low Concentration Ratios.** Initially, CLR01 was found to inhibit the aggregation of IAPP into  $\beta$ -sheet-rich fibrils at an IAPP/CLR01 concentration ratio of 10:1. We asked whether inhibitory activity could be observed at even lower concentrations. To answer this question, we kept IAPP concentration constant and studied the effect of decreasing CLR01 concentrations on IAPP aggregation using ThT fluorescence and electron microscopy (EM).

In the absence of CLR01,  $10 \mu\text{M}$  IAPP displayed a short lag phase followed by a rapid increase in ThT fluorescence indicating formation of  $\beta$ -sheet-rich fibrils (Figure 1C). In contrast, in the presence of an equimolar concentration of CLR01, ThT fluorescence remained at baseline level throughout the duration of the experiment, suggesting complete inhibition of  $\beta$ -sheet formation (Figure 1C), in agreement with data reported previously.<sup>30</sup> As the concentration of CLR01 decreased, a time-dependent increase in ThT fluorescence was observed with kinetics that did not differ significantly from that of IAPP aggregated in the absence of CLR01. However, the final ThT fluorescence levels were substantially lower than those of IAPP alone suggesting partial inhibition of  $\beta$ -sheet formation. Remarkably, this partial

inhibition was observed reproducibly at CLR01 concentrations as low as  $10 \text{ nM}$  (Figure 1C) and even at lower concentrations (see additional results in Supporting Information). Thus, the final ThT fluorescence at IAPP/CLR01 concentration ratio of  $1:10^{-3}$  was  $37 \pm 11\%$  that of IAPP alone. In the presence of equimolar concentration of CLR03, no inhibition was observed, and the final ThT fluorescence was  $107 \pm 2\%$  that of IAPP alone (Figure 1C).

Theoretically, CLR01 might have inhibited ThT binding to IAPP fibrils or quenched ThT fluorescence without affecting IAPP aggregation itself.<sup>35</sup> Therefore, we examined the effect of CLR01 on IAPP fibril formation by EM (Figure 1). At  $t = 0$ , IAPP incubated in the absence or presence of MTs was predominantly amorphous. Following 24 h of incubation in the absence of MTs or in the presence of CLR03, IAPP showed abundant fibrils (Figure 1H, K), whereas in the presence of CLR01 concentrations ranging from  $10 \mu\text{M}$  to  $10 \text{ nM}$  (Figure 1I, J), the morphology was predominantly amorphous with occasional observation of thin, thread-like immature fibrils (e.g., Figure 1J). These immature fibrils were observed only in some experiments and their observation did not correlate with CLR01 concentration. These drastic differences between the effects of CLR01 and CLR03 supported the idea that inclusion of K and/or R residues inside the cavity of CLR01 was the basis of the observed inhibition of aggregation.

Next, we asked whether excess CLR01 could disaggregate IAPP fibrils, similarly to results obtained previously with amyloid  $\beta$ -protein<sup>30</sup> and  $\alpha$ -synuclein.<sup>36</sup> IAPP ( $10 \mu\text{M}$ ) was

allowed to aggregate under similar conditions to those described above, yet for these experiments, the reaction mixtures were not shaken in order to slow down the kinetics so the reaction could be followed more accurately. Under these conditions, the lag phase was extended to  $\sim 2$  h, following which the ThT fluorescence increased gradually over the next 72 h and then plateaued. CLR01 was added at two different time points. The first was at 7 h, during the exponential increase phase, when immature fibrils were expected to exist in the reaction (D1), and the second was at 170 h, after the fibrils presumably had sufficient time to mature (D2). All three reactions were followed up to 500 h.

In the absence of CLR01, following the initial exponential growth phase, little change was observed in the ThT fluorescence for the remainder of the experiment (500 h, Supplementary Figure S2). Morphological examination showed a mixture of short fibrils ( $96 \pm 51$  nm long, 8–9 nm diameter), and globular oligomer ( $19 \pm 5$  nm diameter) at  $t = 0$  h (Supplementary Figure S2). After 7 h of incubation, the fibrils appeared to elongate ( $343 \pm 271$  nm long, 8–9 nm diameter), and only a few globular oligomers ( $22 \pm 5$  nm diameter) were still apparent. By 170 h, the IAPP samples showed a dense mesh of mature, indefinite-length fibrils (Supplementary Figure S2).

Addition of CLR01 at  $t = 7$  h, during the exponential-growth phase, halted the sharp increase in ThT fluorescence in reaction D1 at  $\sim 30\%$  of the final value of IAPP alone. During the next 3 weeks, the fluorescence increased slowly up to  $\sim 40\%$  by 500 h. EM examination showed fibrils that were shorter and less abundant than those in the control reaction in the absence of CLR01 (Supplementary Figure S2).

Addition of CLR01 to mature fibrils at  $t = 170$  h in reaction D2 caused a rapid decline of the fluorescence to  $\sim 55\%$  within the next 24 h, following which the fluorescence slowly increased to  $\sim 70\%$  by 500 h. Similarly to reaction D1, the fibrils in reaction D2 were shorter and their density was substantially lower than in the control reaction (Supplementary Figure S2). These data suggest that CLR01 may disaggregate a relatively loose component of the mature fibrils, whereas a presumably more tightly arranged core of the amyloid fibrils remains and does not disaggregate.

**CLR01 Modulates the Secondary-Structure Transition of IAPP.** To explore further the effect of CLR01 on the self-assembly process of IAPP, we studied its impact on conformational changes during this process using far-UV circular dichroism (CD) spectroscopy. IAPP was incubated in the absence or presence of MTs, and CD spectra were recorded for up to 24 h (Figure 2). To keep the data consistent with the ThT and EM experiments, IAPP concentration was kept at 10  $\mu\text{M}$ . Under these conditions, the signal-to-noise ratio was suboptimal. Consequently, multiple attempts to deconvolute the spectra using several deconvolution programs and protein data sets did not yield meaningful data. Therefore, the analysis presented here is qualitative.

In the absence of MTs, the initial spectrum of IAPP was characterized by a minimum at 201 nm and an inflection at 222 nm, suggesting that IAPP was primarily in a statistical coil conformation, possibly with a minor contribution of  $\alpha$ -helix. This conformational state reflects the fact that IAPP was disaggregated by treatment with hexafluoroisopropanol (HFIP) prior to its incubation in buffer, a necessary step for reproducible measurement. However, this state likely does not reflect the physiologic conformation of IAPP monomers,

which have been reported to have a higher  $\alpha$ -helical content.<sup>9,37</sup> Following 1 h of incubation, the minimum at 201 nm decreased in intensity, a local maximum developed at 208 nm, and a minimum developed at 220 nm, suggesting formation of a mixture containing both  $\alpha$ -helix and  $\beta$ -sheet structures.<sup>38</sup> With continued incubation, the maximum at 208 nm increased in intensity and shifted slightly toward shorter wavelengths. By 24 h, this maximum was a prominent feature at 203 nm. Concomitantly, the minimum at 222 increased in (negative) intensity. Correlation between the CD (Figure 2A) and EM (Figure 1H) data showed that by 24 h, the IAPP preparation still contained a mixture of  $\alpha$ -helical and  $\beta$ -sheet conformations despite formation of abundant fibrils. The spectra had an isodichroic point at 217 nm, suggesting that although both the initial and final spectra were characterized by high content of more than one structural feature, the conformational transition occurred between two predominant states without significant accumulation of intermediates. In agreement with formation of large aggregates, we observed particulate material in these samples at 24 h by the naked eye.

In the presence of equimolar concentration of CLR01, the initial spectrum was similar to that of IAPP alone. Within 1 h of incubation, two minima developed at 203 and 222 nm, suggesting high  $\alpha$ -helix content. The intensity of the entire spectrum decreased gradually with incubation. In contrast to IAPP alone, the solutions of these reactions remained clear for the entire duration of the experiment, suggesting that the decrease in intensity reflected *bona fide* conformational changes rather than loss of material. By 24 h, the spectrum had a global minimum at 217 nm, possibly a local minimum at 222 nm, and a maximum at 191 nm, suggesting an increased portion of  $\beta$ -sheet character in the  $\alpha/\beta$ -structure mixture (Figure 2B).

Interestingly, at the IAPP/CLR01 concentration ratio of  $1:10^{-3}$ , respectively (Figure 2C), though qualitatively the initial spectrum was similar to that of IAPP in the absence of CLR01, the minimum at 201 nm had  $\sim 1.6$  times higher intensity than in the spectrum of IAPP alone or of IAPP in the presence of equimolar CLR01 concentration. This increase in signal intensity suggests rapid induction of a conformational change in IAPP by low concentrations of CLR01. Upon incubation, the intensity of this minimum decreased, and by 24 h, a global minimum was observed at 220 nm. Concomitantly, the portion of the spectrum between 190–206 nm shifted toward positive molar ellipticity, suggesting an increase in  $\beta$ -sheet character. No isodichroic point was observed in the presence of CLR01 at any concentration, suggesting that the conformational transition involved accumulation of intermediates, likely characterized by increased  $\alpha$ -helical character. In contrast to IAPP alone, no particulate material or precipitate was observed in any of the IAPP/CLR01 mixtures.

Because CLR01 appeared to facilitate formation of  $\alpha$ -helical structures at  $[\text{CLR01}] \leq [\text{IAPP}]$ , we asked whether excess CLR01 would further stabilize such structures. In the presence of 10-fold excess CLR01 (Figure 2D), the initial IAPP spectrum was similar to the one in the absence of CLR01 (Figure 2A). Within 1 h, the spectrum changed to one characterized by minima at 208, 218, and 222 nm, suggesting a conformational mixture dominated by  $\alpha$ -helices. The spectrum appeared to be stable, except for a small decrease in intensity up to 24 h, suggesting that CLR01 indeed stabilized  $\alpha$ -helical structures.

In the presence of an equimolar concentration of CLR03, the initial spectrum was characterized by a minimum at 201 nm with intensity  $\sim 1.6$  times higher than that of IAPP alone,

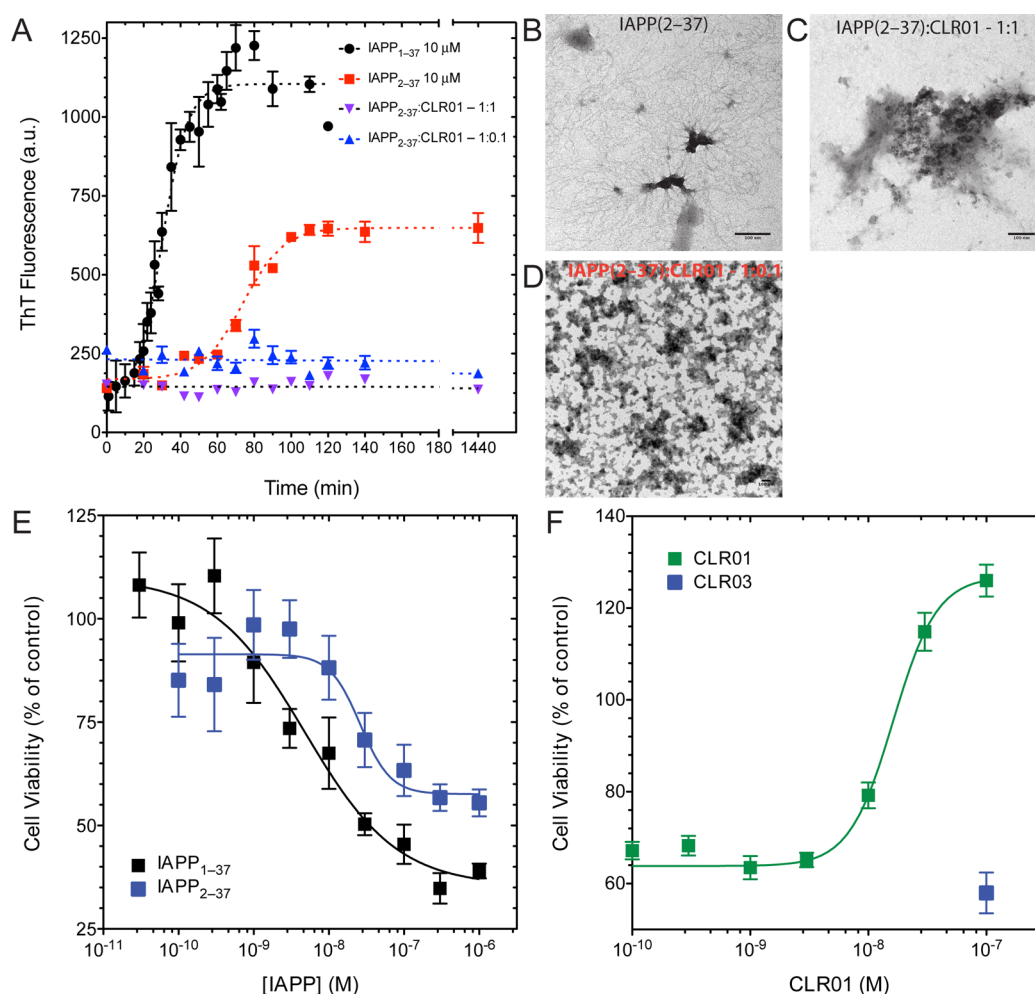


**Figure 3.** K1 is not necessary for inhibition of IAPP aggregation and toxicity by CLR01. For aggregation assays, 10  $\mu\text{M}$  IAPP<sub>2-37</sub> was incubated in the absence or presence of equimolar concentration of CLR01 at 25 °C with constant agitation. (A) Formation of  $\beta$ -sheet was monitored by the ThT fluorescence assay. IAPP<sub>1-37</sub> is shown for comparison. The data are mean  $\pm$  SEM of six independent experiments. (B–D) The morphology of 10  $\mu\text{M}$  IAPP<sub>2-37</sub> incubated in the absence (B) or presence of 10  $\mu\text{M}$  (C) or 1  $\mu\text{M}$  (D) of CLR01 was examined by EM. The images are representative of three independent experiments. Scale bars denote 100 nm. (E) RIN5fm cells were incubated with increasing concentrations of IAPP<sub>1-37</sub> or IAPP<sub>2-37</sub> for 24 h, and cell viability was measured using the MTT assay. The data are presented as mean  $\pm$  SEM of six experiments with four wells per data point ( $n = 24$ ). (F) IAPP<sub>2-37</sub> (100 nM) in the presence of increasing CLR01 concentrations was incubated with cultured RIN5fm  $\beta$ -cells for 16 h, and cell death was measured using the MTT assay. CLR03 was used as a negative control. The results are an average of three to six experiments with three wells per data point ( $n = 9$ –18) and are represented as mean  $\pm$  SEM.

similar to the spectra observed in the presence of 10 nM CLR01. However, in contrast to the low concentrations of CLR01, the spectrum changed within 4 h to one characterized by an intense maximum at 202 nm and a minimum at 222 nm, suggesting a mixture dominated by  $\beta$ -sheet (note the different scale in Figure 2E compared to Figures 2A–D). This spectrum remained unchanged by 24 h. These data are in agreement with the moderately higher intensity of ThT (Figure 1C) and fibril abundance (Figure 1K) of IAPP in the presence of CLR03 compared to IAPP alone and with recent data suggesting that CLR03 moderately accelerates A $\beta$  aggregation.<sup>39</sup>

**CLR01 Protects RIN5fm  $\beta$ -Cells against IAPP-Induced Apoptosis.** Previously, we found that CLR01 protected RIN5fm cells from IAPP-induced toxicity using the MTT reduction assay with half-maximal inhibition ( $\text{IC}_{50}$ ) =  $6 \pm 3$   $\mu\text{M}$ .<sup>30</sup> MTT reduction is a common cell viability assay, which measures mitochondrial activity rather than cell death *per se*.<sup>40</sup> IAPP is known to cause  $\beta$ -cell death predominantly by inducing apoptosis.<sup>21,41</sup> To test whether CLR01 protected cells against

IAPP-induced apoptosis, we incubated RIN5fm cells with IAPP in the absence or presence of CLR01 and measured cytoplasmic histone-associated nucleosomes, which are early indicators of apoptotic cell death.<sup>42</sup> As shown in Supplementary Figure S3A, IAPP induced apoptosis in RIN5fm cells dose-dependently, increasing apoptosis above baseline level by  $18 \pm 4\%$  at 0.3  $\mu\text{M}$  and by  $64 \pm 2\%$  at 1.0  $\mu\text{M}$ , following 16 h of treatment. Similar to the results observed previously using the MTT assay,<sup>30</sup> CLR01 inhibited IAPP-induced apoptosis in RIN5fm cells completely at IAPP/CLR01 concentration ratio of 1:100, respectively (Supplementary Figure S3B).

**CLR01 Inhibits IAPP Aggregation and Toxicity in the Absence of K1.** The surprising capability of CLR01 to modulate IAPP aggregation at concentration ratios  $\leq 1:1000$  and the observation that much higher concentrations were needed for inhibiting IAPP-mediated cytotoxicity led us to explore further the mode of interaction of CLR01 with IAPP. Specifically, we wondered if contacts other than the predicted binding to K1, which we did not expect to have a strong impact

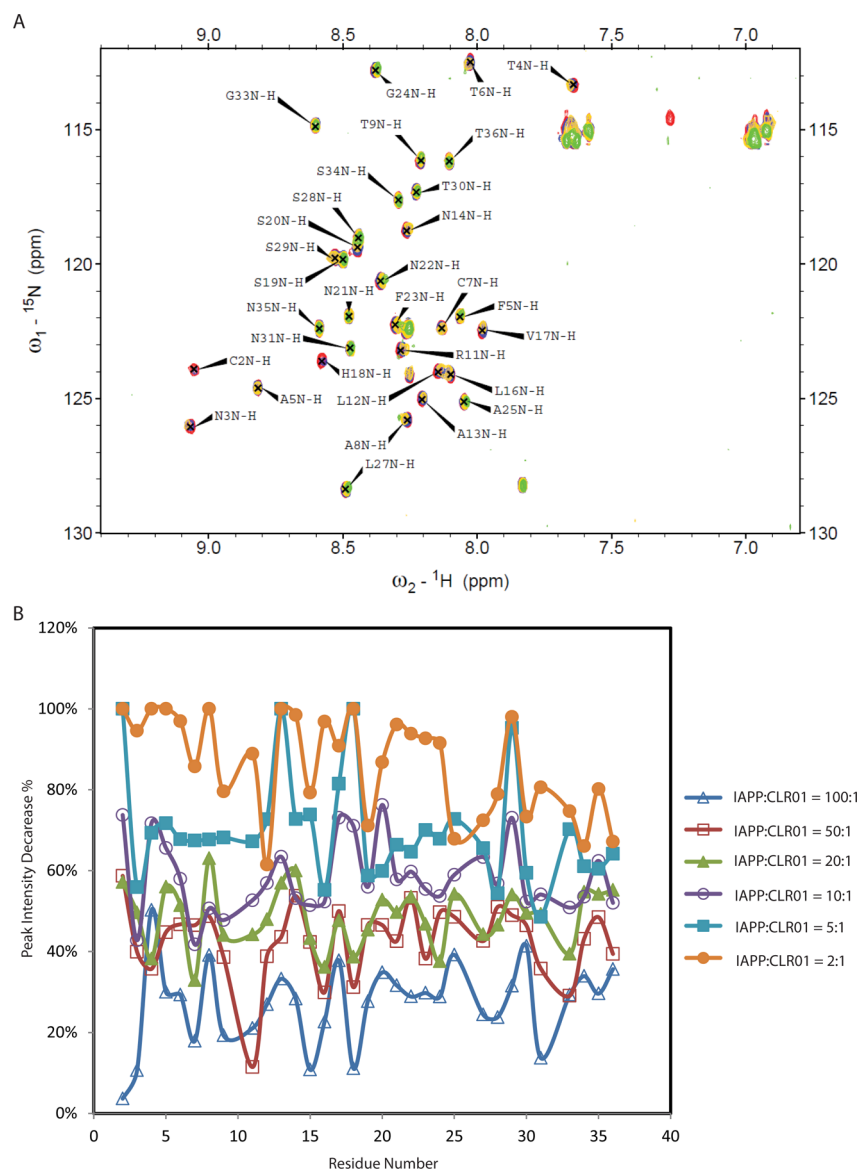


**Figure 4.** Substoichiometric amounts of CLR01 induce a global conformational rearrangement in IAPP. IAPP (100  $\mu$ M) was incubated at 4  $^{\circ}$ C in 50 mM potassium phosphate, 100 mM potassium chloride, pH = 5.5. CLR01 was prepared as a 24.5 mM stock solution and titrated in at the indicated concentration ratios. (A) Color key: IAPP alone – red; IAPP/CLR01 = 1:0.1 – blue; IAPP/CLR01 = 1:0.2 – yellow; IAPP/CLR01 = 1:0.5 – green. (B) Percent peak intensity decrease in IAPP  $^1$ H– $^{15}$ N HSQC spectra upon the addition of increasing concentrations of CLR01. Not all the concentrations shown in panel B were included in panel A for clarity.

on IAPP aggregation, might be involved in the unexpected behavior we observed. First, we asked whether binding to K1 was at all important for CLR01 inhibition of IAPP aggregation and/or toxicity. To answer this question, we investigated the effect of CLR01 on IAPP<sub>2–37</sub>. We incubated the N-terminally truncated IAPP analogue under the same conditions used for full-length IAPP and measured temporal changes in ThT fluorescence, morphology, and cell viability.

A time-dependent increase in ThT fluorescence suggested that in the absence of MTs, IAPP<sub>2–37</sub> formed  $\beta$ -sheet-rich aggregates, though the kinetics of aggregation was slower, and the final ThT fluorescence intensity was approximately half that of IAPP<sub>1–37</sub> (Figure 3A). Following 24 h of incubation, IAPP<sub>2–37</sub> formed abundant thin, thread-like curvilinear structures (Figure 3B). These results demonstrated that interactions involving K1 play an important role in IAPP self-assembly. Intriguingly, despite the removal of the putative

binding site at K1, CLR01 was found to completely abolish the  $\beta$ -sheet and thread-like structure formation of IAPP<sub>2–37</sub> at IAPP<sub>2–37</sub>/CLR01–1:1 or 10:1 concentration ratios (Figure 3A, C, D). Thus, in the presence of CLR01, no increase in ThT fluorescence was observed, and only amorphous structures were detected following 24 h of incubation.

Using the MTT assay in RINSfm  $\beta$ -cells, IAPP<sub>2–37</sub> was found to be  $\sim$ 7 times less toxic than IAPP<sub>1–37</sub> ( $EC_{50} = 5 \pm 5$  nM) decreasing cell viability in a dose-dependent manner with an  $EC_{50}$  of  $37 \pm 52$  nM (Figure 3E). Consistent with the ThT and EM data, CLR01, but not CLR03, protected the cells against IAPP<sub>2–37</sub>-induced toxicity (Figure 3F) despite the absence of the K1 binding site. Surprisingly, the  $IC_{50}$  for CLR01-mediated inhibition of toxicity induced by 100 nM IAPP<sub>2–37</sub> was  $16 \pm 4$  nM. This finding supports a direct role for K1 in IAPP toxicity because it demonstrates that whereas the toxicity of IAPP<sub>1–37</sub> requires a large excess of CLR01 for inhibition, substoichiometric

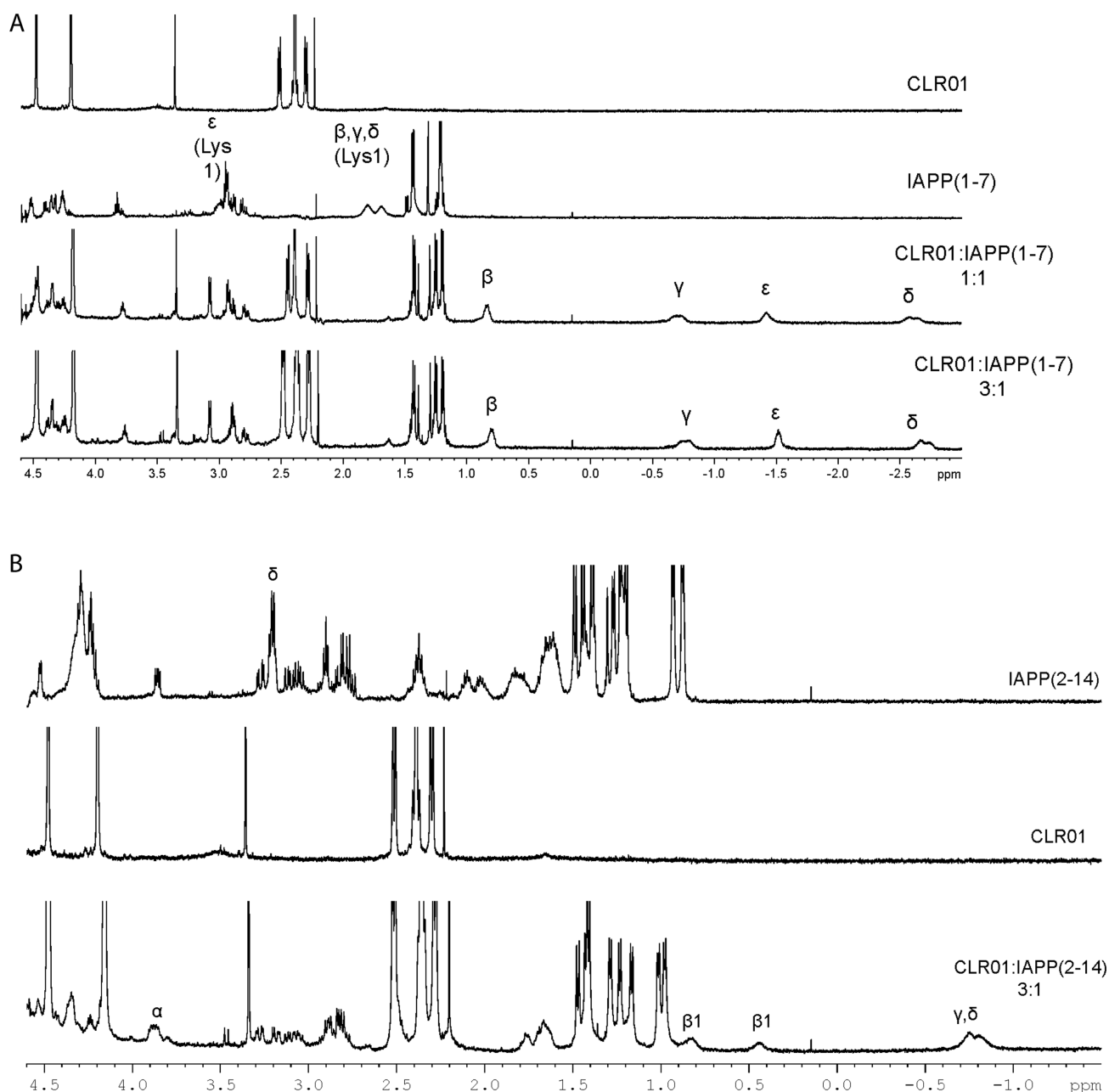


**Figure 5.** CLR01 includes K1 and R11 inside its cavity. (A) IAPP<sub>1-7</sub>, CLR01, and their 1:1 or 1:3 complexes in 10 mM phosphate-buffered D<sub>2</sub>O, pH 7.2. The K1 side-chain methylene signals are assigned as  $\alpha$ ,  $\beta$ ,  $\gamma$ ,  $\delta$  and  $\epsilon$ . All the methylene resonances, most notably the  $\delta$ - and  $\epsilon$ -protons, are shifted upfield by 4.4 and 4.5 ppm, respectively, indicating strong binding of CLR01 to K1. (B)  $^1\text{H}$  NMR of IAPP<sub>2-14</sub>, CLR01, and their 1:3 complex in 10 mM phosphate-buffered D<sub>2</sub>O, pH 7.2. The R11 side-chain methylene signals are assigned as  $\alpha$ ,  $\beta$ ,  $\gamma$ , and  $\delta$ . The  $\delta$ -protons are shifted upfield by  $\sim$ 4 ppm, indicating strong binding of CLR01 to R11.

metric CLR01 concentrations are sufficient for inhibition of the weaker toxicity of IAPP<sub>2-37</sub>. Taken together, the data obtained with IAPP<sub>2-37</sub> strongly supported the existence of an additional binding site on IAPP for CLR01.

#### Investigation of CLR01's Binding Sites on IAPP.

Investigating the binding site(s) of CLR01 on IAPP was important not only because of the inhibition of aggregation and toxicity of IAPP<sub>2-37</sub> but also because a previous study showed that CLR01 might have two different binding modes. When the complex of CLR01 with the small adapter protein, 14-3-3, was investigated by X-ray crystallography,<sup>43</sup> two binding modes were found at different positions. The expected binding mode in which the K side chain threaded through the tweezer's cavity,

and weaker binding involving only formation of ion-pairs between a phosphate group in CLR01 and the  $\epsilon$ -NH<sub>3</sub> group of the K side chain. Here, we attempted first to identify the binding site(s) of CLR01 on IAPP, by examining mixtures of uniformly  $^{15}\text{N}$ -labeled IAPP and CLR01 by solution-state NMR. For simplicity, these experiments used a non-native IAPP analogue in which the C-terminal group was a carboxyl rather than a carboxamide. This modification is known to affect the conformation and aggregation of IAPP,<sup>37,44</sup> yet the conformational difference at the relevant residues, K1 and R11, is minor relative to the structure of the native peptide.<sup>45</sup> Our study focused only on a search for a binding site, as was done previously with A $\beta$ .<sup>30</sup> Because binding of CLR01 was

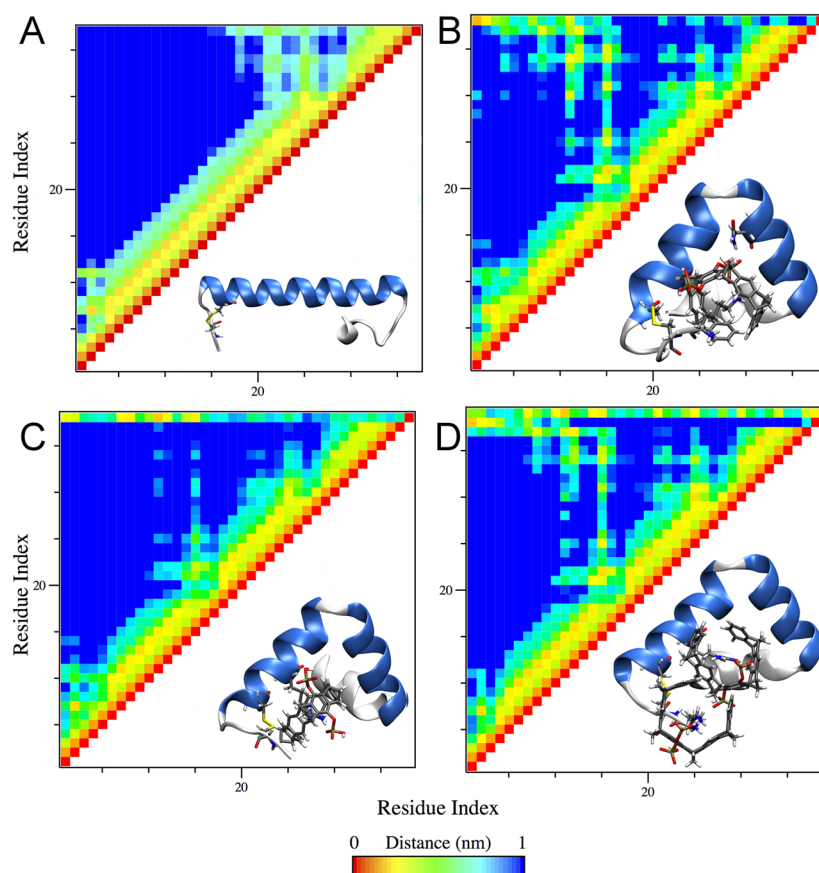


**Figure 6.** IAPP wraps around one or two molecules of CLR01 on K1 and/or R11. (A) IAPP<sub>1–37</sub> adopts an extended conformation with no kink between residues 9 to 25. In both (B) IAPP<sub>1–37</sub>CLR01<sub>K1</sub> and (C) IAPP<sub>1–37</sub>CLR01<sub>R11</sub>, the presence of CLR01 confers preference for a kinked conformation. (D) Two molecules of CLR01 can be accommodated by the kinked IAPP<sub>1–37</sub>CLR01<sub>K1+R11</sub>.

predicted to be at K1 and to a lower extent at R11, the nature of the C-terminal group was not expected to affect the binding substantially.

Under the conditions used for the NMR experiments, the HSQC signal of full-length IAPP was stable for at least 12 h (Supplementary Figure S4). Already upon addition of CLR01 at an IAPP/CLR01 concentration ratio as low as 100:1, substantial perturbation of IAPP resonances was observed (Figure 4). The magnitude of change in chemical shift and peak intensity increased with CLR01 concentration (Figure 4). The decrease in peak intensity likely occurred due to chemical exchange broadening caused by the binding of CLR01. This behavior was consistent with the CD and EM data, which suggested that even at low concentration ratios, CLR01 induced substantial global conformational rearrangement—likely reflecting oligomerization rather than just local perturbation. Consequently, however, the <sup>1</sup>H–<sup>15</sup>N HSQC data could not reveal specific binding sites for CLR01 on IAPP. This is likely because terminal residues, such as K1, are difficult to observe in HSQC experiments due to high exchange rates of the N-terminal amino group protons, and the relatively low affinity binding of CLR01 for R11.

To further elucidate whether CLR01 bound to K1 or R11, in subsequent solution-state NMR experiments, we investigated the binding of CLR01 to unlabeled N-terminal fragments of IAPP. Binding of CLR01 to K1 was probed by adding CLR01 to IAPP<sub>1–7</sub> and monitoring the mixture using 1D- and 2D-NMR (COSY). At an IAPP<sub>1–7</sub>/CLR01–1:1 concentration ratio, all the K side chain methylene signals shifted drastically

upfield into the negative-ppm range (Figure 5A), as shown previously,<sup>33</sup> indicating inclusion of the K1 side chain inside the MT cavity. No further change, except slightly higher peak amplitude, occurred at 3-fold CLR01 excess (Figure 5A and Supplementary Figure S5). Fluorescence titration yielded  $K_d = 8.69 \mu\text{M}$  (Supplementary Figure S6), similar to values reported previously for N-terminal K residues.<sup>46</sup> In contrast, no change was observed in the spectrum of IAPP<sub>2–7</sub> even in the presence of 3-fold excess CLR01 (Supplementary Figure S7), indicating that the presence of K1 was essential for CLR01 binding to IAPP<sub>1–7</sub>.

Binding to R residues has been reported previously to be substantially weaker than to K.<sup>30,33,47</sup> Therefore, we predicted that CLR01 would bind predominantly to K1 rather than to R11 in IAPP. To test whether CLR01 also bound to R11, similar experiments were performed with IAPP<sub>1–14</sub>. In the presence of 3-fold excess CLR01, the side-chain protons of both K1 and R11 showed an upfield shift (Supplementary Figure S8), indicating binding at both sites. As expected, the shift of R11 proton resonances appeared weaker than that of K1 protons in the spectrum of IAPP<sub>1–14</sub>, yet peak overlap made analysis of the spectrum difficult. Therefore, we examined CLR01's affinity for R11 in IAPP<sub>2–14</sub>, where unambiguous binding of CLR01 to R11 was observed (Figure 5B and Supplementary Figure S9). Fluorescence titration revealed that CLR01 complexation at R11 occurred with  $K_d = 104 \mu\text{M}$  (Supplementary Figure S10), an order of magnitude weaker than at K1. Taken together, the NMR and fluorescence data strongly supported predominant CLR01 binding to K1 and the

existence of a second binding site at R11. The latter observation provided a plausible explanation for the inhibition of IAPP<sub>2–37</sub> aggregation and toxicity by CLR01 (Figure 3), yet did not reveal how CLR01 might have affected IAPP assembly at low concentration ratios. To investigate further the impact of CLR01 binding on the structure of IAPP, we used REMD simulations.

**REMD Simulations of the Interactions between CLR01 and IAPP.** Simulations were carried out on two systems differing in the  $\alpha$ -helical content of the starting conformation of IAPP.

**System I (IAPP<sub>1–37</sub> <sup>$\alpha_{64\%}$</sup> ).** In **System I**, the structure of micelle-bound IAPP<sub>1–37</sub> in its native amidated form, as reported by Nanga et al.<sup>45</sup> ( $\alpha$ -helix content of 51%), was used as a starting point for REMD simulations of IAPP<sub>1–37</sub> in explicit water. We selected this monomer structure on the basis of the availability of reliable structural data in the protein data bank. Though this structure is of micelle-bound IAPP, which was not used in the experiments described above, to the best of our knowledge, due to its high tendency to aggregate, there are no coordinates reported for monomeric human IAPP in aqueous buffer that could be used as a starting point for the simulations. In addition, due to the well-documented role of  $\alpha$ -helical structures in IAPP aggregation,<sup>9,48–51</sup> we thought it was important to investigate the effect of CLR01 on IAPP monomers with this secondary structure present.

The simulations indicated that, unlike in the initial, micelle-bound structure, in water, the central  $\alpha$ -helix in IAPP<sub>1–37</sub> (residues 6–28) adopted an extended conformation (Figure 6A) and that the  $\alpha$ -helix content of this IAPP<sub>1–37</sub> conformer was 64%. The population of structures with fully extended  $\alpha$ -helix represented 96% of the resulting ensemble, whereas only 4% of the structures contained a kink at H18 (cluster population analysis is given in Supplementary Table S1). Throughout the simulations, the central  $\alpha$ -helix and the shorter, C-terminal  $\alpha$ -helical region (shown in white in Figure 6) were conserved, while the C-terminal region 30–37 got closer to residues 17–28. In contrast, R11 and N14 moved away from the C-terminal region, and no interactions were found between the N- and C-terminal regions in the extended structure (Figure 6A).

The REMD simulations of IAPP<sub>x–37</sub> ( $x = 1, 2$ ) in the presence of one or two CLR01 molecules are labeled IAPP<sub>x–37</sub>CLR01<sub>K1</sub>, IAPP<sub>x–37</sub>CLR01<sub>R11</sub>, or IAPP<sub>x–37</sub>CLR01<sub>K1+R11</sub> for trajectories in which CLR01 was placed initially on K1, on R11, or on both residues, respectively. In all cases, throughout the simulations, the side chains of K1 and/or R11 remained inside the tweezer's cavity, in agreement with the NMR experiments (Supplementary Table S2). The introduction of CLR01 resulted in important conformational changes in IAPP<sub>1–37</sub>. In all cases, the kinked structure was favored representing 100%, 95%, and 100% of the ensembles obtained for IAPP<sub>1–37</sub>CLR01<sub>K1</sub>, IAPP<sub>1–37</sub>CLR01<sub>R11</sub>, and IAPP<sub>1–37</sub>CLR01<sub>K1+R11</sub>, respectively (Figures 6B–D, Supplementary Table S1).

Although in REMD simulations the system can escape from local minima<sup>52</sup> and we achieved convergence of the populations, we asked whether CLR01 binding would not only stabilize the initial kink at H18 in IAPP but also might induce formation of this kink if the simulations started from the extended  $\alpha$ -helix conformation. REMD simulations of IAPP<sub>1–37</sub>CLR01<sub>K1</sub> starting from the extended conformation showed a slow conversion to the kinked form. After 60 ns, the

kinked conformation represented 12% of the entire population with a tendency to increase. This value was 3 times higher than in simulations of IAPP<sub>1–37</sub> alone, suggesting that with sufficiently long simulation time, CLR01 binding would have converted IAPP from the extended conformation to predominantly the kinked one.

The contact maps in Figure 6B,C reveal subtle differences between the simulations in which CLR01 was placed initially on K1 or on R11. When placed initially on K1, CLR01 interacted mainly with residues 1 to 15 and did not interact with the C-terminal region. IAPP appeared to wrap around itself while CLR01 was positioned on the plane above the peptide. In contrast, when initially placed on R11, close to the middle of the  $\alpha$ -helix, CLR01 interacted with the entire peptide. Positioning of CLR01 on R11 effectively hindered the interactions between the C- and N-terminal regions. Only R11 and N14 remain somewhat close to the C-terminus. Simulations of IAPP with two tweezers showed a very similar behavior to the simulations with single CLR01 molecules: IAPP was wrapped around the tweezer bound to R11, whereas the CLR01 bound to K1 remained in the plane above the CLR01<sub>R11</sub>–IAPP<sub>1–37</sub> complex (Figure 6D and Supplementary Movies 1A–C).

The simulations of IAPP<sub>1–37</sub> in explicit water in the absence or presence of CLR01 thus indicate that at both 1:1 and 2:1 CLR01/IAPP ratio, respectively, CLR01 forms stable complexes with IAPP<sub>1–37</sub>, in which K1 and/or R11 are included inside the tweezer's cavity, resulting in important conformational changes in the peptide. In the absence of CLR01, IAPP<sub>1–37</sub> adopts an extended conformation, whereas, when CLR01 is added, the kinked conformation dominates. This is especially interesting in view of the NMR work of Lazo and co-workers, who reported that IAPP<sub>11–25</sub> structures with an induced kink in the central region were not aggregation prone.<sup>51</sup> Thus, stabilization of the kink in IAPP<sub>1–37</sub> by CLR01 provides a plausible structural explanation for the inhibition of aggregation by the molecular tweezer.

In IAPP<sub>2–37</sub>, REMD simulation showed that structures with at least one kink between residues 5 and 29 were the most populated (Supplementary Figure S10), in agreement with the lower aggregation propensity of truncated IAPP<sub>2–37</sub> compared to IAPP<sub>1–37</sub>. The central and C-terminal  $\alpha$ -helices were less structured than in IAPP<sub>1–37</sub> (cf. Figure 6A and Supplementary Figure S10). IAPP<sub>2–37</sub> formed more compact structures than IAPP<sub>1–37</sub>, in which Y37 was found closer to residues R11 and N14, whereas the interaction between the C-terminal region and residues 17 to 25 was lost (Supplementary Figure S10). No significant interactions between the N- and the C-terminal regions were found.

The simulations of IAPP<sub>2–37</sub>CLR01<sub>R11</sub> showed a very similar behavior to IAPP<sub>1–37</sub>CLR01<sub>R11</sub>. An interesting difference was that in IAPP<sub>2–37</sub>, the terminal regions became closer upon addition of CLR01 as shown by the increased number of contacts between Y37 and residues 3–15 and between R11 and N14 and residues 25–37 (Supplementary Figure S10).

**System II (IAPP<sub>1–37</sub> <sup>$\alpha_{27\%}$</sup> ).** To further investigate the effect of the tweezers on IAPP<sub>1–37</sub> conformers with less helical content than **System I**, we also studied **System II** (IAPP<sub>1–37</sub> <sup>$\alpha_{27\%}$</sup> ). This IAPP<sub>1–37</sub> conformer was chosen from preliminary REMD simulations performed on an IAPP<sub>1–37</sub> dimer, in which a monomer had an initial 27%  $\alpha$ -helical content (Supplementary Figure S11).

We found that, similarly to **System I**, two kinds of conformations were observed for IAPP<sub>1–37</sub> and

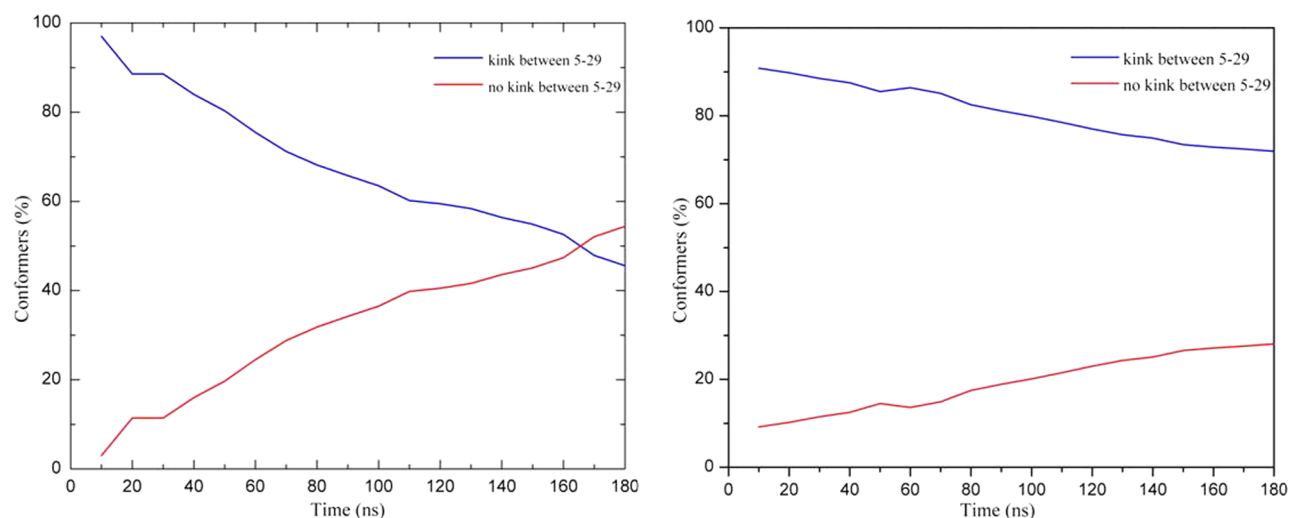


**Figure 7.** CLR01 stabilizes a kinked conformation in structures with lower  $\alpha$ -helical content. Time-dependent conformational change in the kinked (blue) and extended (red) structures found in **System II**, REMD simulations of IAPP<sub>1–37</sub> (left) and IAPP<sub>1–37</sub>CLR01<sub>K1</sub> (right) at 300 K.

IAPP<sub>1–37</sub>CLR01<sub>K1</sub> in **System II**: a kinked conformation interrupting the central  $\alpha$ -helix, and a fully extended  $\alpha$ -helical conformation. Initially, structures with at least one kink between residues 5 and 29 (Figure 7) were the most populated in both cases, in the absence or presence of CLR01, which would be expected considering that the initial geometry contained a kink (Supplementary Figure S11B). However, in agreement with the results obtained for **System I**, the population of kinked structures rapidly decreased in IAPP<sub>1–37</sub>, while the population of extended conformers increased (Figure 7). After 160 ns, in the absence of CLR01, the preferred structure of IAPP<sub>1–37</sub> was the extended conformation. As in **System I**, when the tweezer was placed around K1, the kinked structure dominated with respect to the extended conformation and both populations tended to stabilize at  $\sim$ 140 ns. The side chain of K1 remained inside the tweezer's cavity during the entire REMD simulations (Supplementary Table S2).

Comparison of the REMD simulations in **System I**, in which the structure of IAPP<sub>1–37</sub> in water had 64%  $\alpha$ -helical content and **System II**, in which the  $\alpha$ -helical content was only 27%, clearly showed that in both cases IAPP preferentially formed an extended conformation on its own, whereas binding of CLR01 stabilized a kinked conformation. These data suggest that CLR01 prevents IAPP aggregation by stabilizing a kinked conformation that has been reported previously to be less prone to aggregation.<sup>51</sup>

**Evaluation of Plasma Levels of CLR01 *In Vivo*.** In both the MTT assay<sup>30</sup> and apoptosis assay described above (Supplementary Figure S2), CLR01 protected the cells at an IAPP/CLR01 concentration ratio of  $\sim$ 1:100. IAPP normally is found in the blood circulation at 3–5 pM in humans.<sup>53,54</sup> Elevation of plasma glucose leads to an immediate rise in endogenous plasma IAPP levels to 15–20 pM<sup>55</sup> with  $\sim$ 15 min half-life.<sup>56</sup> Based on these numbers, to inhibit IAPP-induced toxicity, CLR01 might need to achieve plasma concentrations in the low nM range (though *in vitro* stoichiometry does not always accurately predict efficacious *in vivo* doses, see Discussion). To evaluate whether CLR01 could reach the estimated concentration ratio *in vivo* without causing overt toxicity, we administered CLR01 continuously at 1 mg/kg/day to wild-type C57Bl/6 mice for 21 days using subcutaneously implanted osmotic minipumps. The plasma concentration of

CLR01 was measured at 7, 14, and 21 day (Figure 8) and was found to be  $\sim$ 140 nM at steady-state. During the entire period

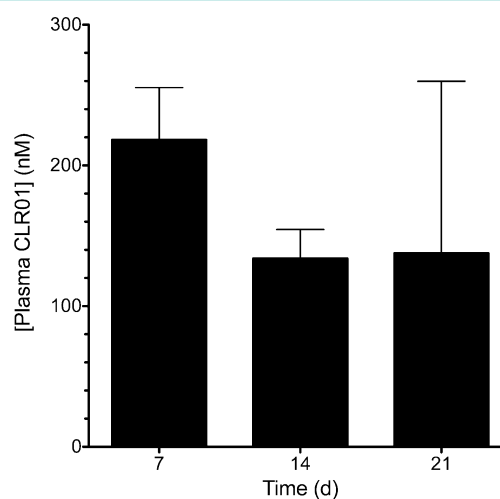


**Figure 8.** CLR01 maintains sufficient plasma level in mice without apparent toxicity. CLR01 was administered subcutaneously to 7–10-wk old, male WT mice for 7–21 d (3 mice per time point) using osmotic minipumps. At each time point, plasma was collected and CLR01 concentration was quantified by HPLC-MS/MS by interpolation into a standard curve.

of the experiment, the mice appeared and behaved completely normally and did not show any side effects, such as lethargy, weight loss, appetite loss, morbidity, or mortality, in agreement with a recently reported efficacy study using a similar dose<sup>57</sup> and a toxicity study in which CLR01 was administered daily at 10 mg/kg/day and was found to have a high safety margin.<sup>58</sup> These results suggest that CLR01 can be administered to mice and achieve sufficient plasma concentrations for inhibition of IAPP toxicity *in vivo* without causing safety concerns.

CLR01 is an artificial receptor for K residues found to be an effective inhibitor of assembly and toxicity of multiple amyloidogenic proteins *in vitro*<sup>30,31,59</sup> and *in vivo*.<sup>36,57,60</sup> The mechanism of action of CLR01 involves micromolar-affinity binding to K residues and interfering with hydrophobic and electrostatic interactions that are important for the initial self-

assembly of amyloidogenic proteins and/or their interaction with cellular targets.<sup>30,58,61,62</sup>

Initially, we found that CLR01 inhibited formation of  $\beta$ -sheet-rich IAPP fibrils and IAPP-induced toxicity. However, although we observed complete inhibition of aggregation at IAPP/CLR01 concentration ratio 10:1, inhibition of toxicity required a ratio of  $\sim$ 1:100, suggesting that blocking the formation of  $\beta$ -sheet-rich aggregates was not sufficient for inhibition of IAPP toxicity.<sup>30</sup> Intrigued by these findings, we investigated further the binding sites for CLR01 in IAPP and the effect of CLR01 binding on IAPP conformation and assembly.

Our ThT and EM data (Figure 1) showed that CLR01 inhibited IAPP  $\beta$ -sheet and fibril formation at unexpectedly low concentrations. Partial inhibition was observed at 10 nM CLR01, 3 orders of magnitude lower than the IAPP concentration used (10  $\mu$ M), and potentially at even lower concentrations (See Supplementary Results and Supplementary Figure S1). These findings were highly surprising and suggested strong modulation of the nucleation step in IAPP aggregation by CLR01. One explanation of these findings is that the interaction of CLR01 with IAPP leads to formation of an alternative nucleus, which rapidly recruits additional monomers into nonfibrillar assemblies. Though proving the existence of such nuclei is difficult—due to the very low abundance of these hypothetical structures on the background of IAPP monomers and oligomers as well as the inability of current experimental methods to provide high-resolution information on IAPP oligomers—several lines of evidence support this hypothesis.

The CD spectra of IAPP in the presence of low, substoichiometric concentrations of CLR01 were distinct from the spectrum of IAPP alone even at the earliest time points measured (Figure 2 and Supplementary Figure S1). Major perturbations in the HSQC spectra of <sup>15</sup>N-labeled IAPP occurred already in the presence of 1 mol % of CLR01 (Figure 4), indicating a global conformational change of the peptide. Complexation was confirmed independently by NMR (Figure 5) and fluorescence (Supplementary Figures S6, S10) titrations of IAPP fragments with CLR01, in which the resulting  $K_d$  value corresponded well with those of isolated K derivatives, and concomitant drastic upfield shifts of K methylene resonances documented the insertion of the K side chain inside the tweezer's cavity. Finally, modeling the conformation of IAPP clearly shows that distinct structures form in the absence of CLR01 than in its presence.

The combination of the modeling with structural (Figures 1,2) and cell toxicity data (Supplementary Figure S3 and ref 30) suggests existence of at least three distinct, putative assembly processes of IAPP: In the absence of CLR01, IAPP monomers adopt an extended structure, possibly rich in  $\alpha$ -helix (Figure 6A), though enrichment of this secondary structure requires lipid membranes, which were not used here. The extended structure is capable of associating with other monomers and serving as a nucleus for aggregation. Upon interaction with other monomers, first toxic oligomers form, which subsequently transform into  $\beta$ -sheet-rich fibrils. In the presence of substoichiometric CLR01 concentrations, CLR01 binds to K1 on IAPP leading to stabilization of a kink at H18 (Figure 6B). Presumably, this conformation also serves as a nucleus for self-assembly. The assemblies formed in this case are toxic, yet they do not convert into amyloid fibrils. In the presence of excess CLR01, binding occurs to both K1 and R11 (Figure 6D) leading to a conformation in which IAPP wraps

itself around the central CLR01 molecule. This structure appears to be nucleation-incompetent and nontoxic.

One of the common mechanisms proposed for amyloid formation is nucleation-dependent polymerization,<sup>63</sup> which means that a monomer or a small oligomer of an amyloidogenic protein serves as a nucleus that can induce its own conformation and propagate this conformation in oncoming monomers. A similar mechanism has been implicated in prion infectivity, whereby monomeric, normally folded cytosolic PrP<sup>C</sup> is recruited by the abnormally folded scrapie form, PrP<sup>Sc</sup>, and upon joining the aggregate, each PrP<sup>C</sup> monomer changes its conformation to that of PrP<sup>Sc</sup>. Recently, formation of toxic aggregates by several amyloidogenic proteins has been reported to be transmissible, similar to prion proteins.<sup>64</sup> We suggest that a similar mechanism may explain the data observed here. Ostensibly, upon binding of CLR01 to an IAPP monomer, the conformation of the peptide changes to one that can recruit additional monomers into a growing assembly. However, this assembly appears to be distinct from typical amyloid. It does not have fibrillar morphology, and its  $\beta$ -sheet content is lower than in amyloid, with a concomitant higher  $\alpha$ -helix content. Nonetheless, our data suggest that at  $[\text{CLR01}] \leq [\text{IAPP}]$ , the IAPP/CLR01 complexes that form serve as nuclei, propagating their conformation in recruited monomers.

Interestingly, although the structure of the IAPP/CLR01 complexes at  $[\text{CLR01}] \leq [\text{IAPP}]$  is not that of typical amyloid and actually prevents amyloid formation, it is still a toxic structure, highlighting the fact that diverse amyloidogenic protein oligomers, including those of IAPP, are toxic, and toxicity is not limited to one particular structure. Our data also demonstrate that at  $[\text{CLR01}] > [\text{IAPP}]$ , when two CLR01 molecules bind IAPP, CLR01 effectively inhibits IAPP-induced toxicity. The high molar ratio required, 100:1, respectively, is likely due to the relatively low  $K_d$  of CLR01 to R11 (Supplementary Figure S10) and the need for the two binding sites at K1 and R11 to be occupied simultaneously for efficient toxicity inhibition.

In this context, it is important to note that the stoichiometry needed for inhibition of toxicity in cell culture may not accurately reflect the stoichiometry *in vivo*. This was demonstrated recently in a study of the therapeutic effect of CLR01 in a mouse model of familial amyloidotic polyneuropathy,<sup>57</sup> in which mutant transthyretin (TTR) aggregates and forms amyloid deposits, predominantly in the gastrointestinal tract and the peripheral nervous system. Similarly to the IAPP case, a relatively high CLR01/TTR concentration ratio, 54:1, was needed for half-maximal inhibition of toxicity in cell culture, even though inhibition of TTR aggregation (measured by ThT fluorescence and EM) was achieved at a 1:1 concentration ratio.<sup>30</sup> Nevertheless, in the mouse model, significant reduction of TTR deposition, apoptosis, ER stress, and protein oxidation was achieved at plasma CLR01/TTR concentration ratio  $\approx$ 1:200. These data suggest that *in vivo*, where multiple mechanisms exist for clearance of misfolded proteins, CLR01 binding even at substoichiometric concentration ratios maintains amyloidogenic proteins in a form that is amenable to degradation and clearance.

In summary, a dual mechanism was found for efficient inhibition of IAPP aggregation and toxicity by the molecular tweezer CLR01. Due to the well-known supramolecular recognition profile of molecular tweezers, a combination of various biophysical, spectroscopic, and biochemical data with both full-length and truncated IAPP analogues could be

supported by REMD simulations. The simulations produced a detailed mechanistic picture of the underlying molecular interactions between peptide and inhibitor. Finally, it is important to note that the data presented here suggest that because physiologic IAPP concentrations are in the pM range, effective plasma concentration of CLR01 can be maintained in mice without apparent toxicity, supporting further development of CLR01 as a potential disease-modifying therapy for T2D.

## METHODS

**Reagents and Materials.** Human, full-length IAPP (IAPP<sub>1–37</sub>) was purchased from PolyPeptide Laboratories. IAPP<sub>2–37</sub> was custom-synthesized by AnaSpec or the UCLA Biopolymers Laboratory. Thioflavin T (ThT) and other reagents were from Sigma. Roswell Park Memorial Institute (RPMI) medium and all other cell culture reagents were from Fisher Scientific unless otherwise specified. Water (18.2 MΩ) was filtered and deionized using a Milli-Q purification system (Millipore). CLR01 and a negative control MT derivative, CLR03 (Figure 1B), were prepared as described previously.<sup>30</sup>

**Peptide Preparation.** IAPP<sub>1–37</sub> and IAPP<sub>2–37</sub> were prepared for all experiments by dissolution in 1,1,1,3,3,3-hexafluoroisopropanol (HFIP) as described previously.<sup>65</sup> Dried, HFIP-treated peptide films were stored at  $-20\text{ }^{\circ}\text{C}$  until use. For biophysical experiments, films were dissolved in a minimal volume of 60 mM NaOH followed by dilution with deionized water to half the final volume and then sonicated for 1 min using a Branson model 1510 bath sonicator. Samples then were diluted to the final volume with 20 mM phosphate buffer (PB: sodium phosphate, pH 7.4) in the absence or presence of MTs. For cell culture experiments, peptide films were solubilized in a minimal volume of 60 mM NaOH, diluted in RPMI 1640 cell culture medium in the absence or presence of MTs, and added to the cells. Medium containing the same NaOH concentration was used as a negative control. MT stock solutions were prepared at 10 mM in deionized water and diluted into the peptide solutions at the required concentration.

**ThT Fluorescence Assay.** For aggregation assays, IAPP<sub>1–37</sub> or IAPP<sub>2–37</sub> solutions (10  $\mu\text{M}$ ) in the absence or presence of MTs were incubated at RT with mechanical agitation. At different time points, 30  $\mu\text{L}$  aliquots of the aggregating solution were mixed with 300  $\mu\text{L}$  of 40  $\mu\text{M}$  ThT in 10 mM PB. The fluorescence was measured following a 5 min incubation at  $\lambda_{\text{ex}} = 452\text{ nm}$  and  $\lambda_{\text{em}} = 485\text{ nm}$ , using a Hitachi Instruments F-4500 spectrofluorometer. Nonspecific background fluorescence was subtracted by using appropriate blanks with no protein and the fluorescence values were normalized to the highest value obtained. Data are presented as mean  $\pm$  SEM of at least six independent experiments.

For disaggregation experiments, IAPP was prepared in PB as described above and aliquoted into 96-well plates at 10  $\mu\text{M}$  final concentration. Each well also contained 30  $\mu\text{M}$  ThT. The final volume in each well was 200  $\mu\text{L}$ . The reactions were incubated at  $25\text{ }^{\circ}\text{C}$  without shaking, and fluorescence was monitored with  $\lambda_{\text{ex}} = 420\text{ nm}$  and  $\lambda_{\text{em}} = 485$ . CLR01 (10-fold) was added at 7 or 170 h, and the reactions were monitored up to 500 h. Aliquots (10  $\mu\text{L}$ ) of the reaction mixtures were removed periodically for morphological examination by EM. The data are presented as means  $\pm$  SEM of 1–3 independent experiments with at 3–10 replicates each.

**Electron Microscopy (EM).** Peptide samples were incubated in the absence or presence of MTs as described for the ThT fluorescence measurements. Aliquots were spotted on

glow-discharged, carbon-coated Formvar grids (Electron Microscopy Science), fixed with 2.5% glutaraldehyde, and stained with uranyl acetate as described previously.<sup>66</sup> The samples were analyzed using a JEOL CX 100 transmission electron microscope.

**Circular Dichroism (CD) Spectroscopy.** Peptides were incubated in the absence or presence of MTs, as described for the ThT fluorescence measurements, but in Hellma 1 mm path-length quartz cuvettes. CD measurements were performed using a JASCO J-810 spectropolarimeter as described previously.<sup>67</sup> Briefly, spectra were collected over the wavelength range of 190–260 nm at 0.2 nm intervals with a spectral bandwidth of 0.8 nm and 1 s integration time. Experiments were performed at least four times, and the spectra of representative experiments are shown after subtracting the spectra of buffer alone using OriginLab's Origin 7.

**Apoptosis Assay.** RIN5fm cells were cultured in RPMI media supplemented with 10% fetal bovine serum (FBS), 2 mM L-glutamine, 1 mg mL<sup>-1</sup> D-glucose, 0.1 mM nonessential amino acids, and antibiotics. Cells were plated in 12-well plates at a density of 375 000 cells per well and incubated for 24 h. IAPP in the absence or presence of CLR01 was applied to the cells and incubated for 16 h. Then, cells were detached by treatment with a trypsin-EDTA solution and counted. Apoptosis was assessed using a Roche Diagnostics Cell Death Detection ELISA kit, which measures cytoplasmic histone-associated nucleosomes as early indicators of apoptotic cell death.<sup>42,68</sup>

**Solution-State NMR of Full-Length IAPP.** Uniformly <sup>15</sup>N-labeled IAPP-COOH was obtained from rPeptide. The peptide was dissolved in 1% acetic acid at 2 mg mL<sup>-1</sup>, as suggested by the manufacturer, and then diluted in 50 mM potassium phosphate, 100 mM potassium chloride, pH 5.8, to a final concentration of 100  $\mu\text{M}$ . The pH was adjusted to 5.5. Then, IAPP and CLR01 were mixed slowly to yield concentration ratios ranging from 100:1 to 1:1, respectively. 2D <sup>15</sup>N–<sup>1</sup>H HSQC NMR spectra of freshly prepared <sup>15</sup>N-labeled IAPP samples in the absence or presence of CLR01 were collected at  $4\text{ }^{\circ}\text{C}$  using an 800-MHz Bruker Avance II spectrometer equipped with a cryoprobe. The acquisition time was  $\sim$ 37 min for each HSQC spectrum. Assignments were based on resonances reported previously.<sup>9</sup>

**Replica Exchange Molecular Dynamics (REMD) Simulations.** The initial set of coordinates of micelle-bound IAPP<sub>1–37</sub> in its native amidated form was taken from Nanga et al.<sup>45</sup> (PDB entry 2L86, here called **System I**). Nanga et al.'s structure was used as a starting point for REMD simulations that allowed exploring the conformations of native IAPP in explicit water. To investigate the effect of CLR01 on IAPP<sub>1–37</sub> with lower  $\alpha$ -helix content than **System I**, an additional conformation of IAPP<sub>1–37</sub> was also used as a starting point for REMD simulations (Supplementary Figure S11): a structure with  $\sim$ 27%  $\alpha$ -helical content (**System II**) chosen from preliminary REMD simulations performed by us on an IAPP<sub>1–37</sub> dimer. As in **System I**, extended REMD simulations were performed for **System II** in the absence or presence of CLR01 bound to K1.

The CHARMM27 force field<sup>69</sup> (CMAP corrections included) was used for protein and tweezers. The parameters of CLR01 were obtained with the SwissParam<sup>70</sup> server and tested in a previous study.<sup>71</sup> All the simulations and the analysis of the results were done using GROMACS 4.6.1.<sup>72</sup> Periodic boundary conditions were set and the system was solvated in a

box of TIP3P water<sup>73</sup> and neutralized. The Coulomb interactions were treated by the reaction field approach,<sup>74</sup> and a cutoff of 14 Å was used for both Coulomb and van der Waals interactions. The temperature for the preliminary equilibration MD was set to 290 K. The LINCS algorithm was used for constraining bonds<sup>75</sup> and the Particle Mesh Ewald method, to handle the electrostatic interactions.<sup>76,77</sup>

The temperature range for the REMD simulations was set between 290 and 340 K. The temperature distribution was obtained as described previously by Patriksson and van der Spoel<sup>78</sup> to yield 33–34 replicas, depending of the system. Starting with the equilibrated structure at 290 K, each replica of the system was submitted to 10 ns NVT simulations. After each replica was equilibrated at each temperature, 60 ns NPT REMD simulations<sup>79,80</sup> were performed for **System I** and 180 ns for **System II**.

For the cluster analysis of the trajectories at 300 K, the GROMOS method was used<sup>81</sup> with the backbone of residues 5 to 29 as reference. The resulting clusters were classified according to the presence or absence of a kink in the central  $\alpha$ -helix.

**Measurement of Steady-State CLR01 Concentration in Mouse Plasma.** Experiments were compliant with the National Research Council Guide for the Care and Use of Laboratory Animals and were approved by the UCLA Animal Research Council and the Ethics Committee. C57Bl/6 mice were obtained through the UCLA Surplus Experimental Animal Resource Sharing program. Three, 7–10-week old, male mice were used per time point. CLR01 was administered to the mice continuously, subcutaneously at 1 mg kg<sup>-1</sup> day<sup>-1</sup> via Alzet osmotic minipumps. At 7, 14, and 21 days, the mice were anesthetized with pentobarbital, and the chest cavity was exposed to reveal the heart. A 21-gauge needle connected to a 1-cc syringe was inserted into the right ventricle of the heart, and the blood was slowly withdrawn and immediately transferred to Capiject Li-Heparin gel-barrier tubes as described previously.<sup>60</sup> Plasma was obtained by centrifugation (1250g, 4 °C for 10 min), frozen immediately, and stored at -20 °C. Samples were analyzed using standard HPLC-MS/MS techniques by Wolfe Laboratories Inc., and CLR01 concentration was determined by comparison with duplicate plasma matrix calibration curves over a linear range from 5–5000 ng mL<sup>-1</sup> by interpolation of sample peak area data into the calibration curve.

## ■ ASSOCIATED CONTENT

### ● Supporting Information

Supplement methods and additional data, including fluorescent measurements, decay curves, and NMR spectra, among other data, as noted in the text. This material is available free of charge via the Internet at <http://pubs.acs.org>.

## ■ AUTHOR INFORMATION

### Corresponding Author

\*E-mail: [gbitan@mednet.ucla.edu](mailto:gbitan@mednet.ucla.edu). Phone: 310-206 2082. Fax: 310-206 1700.

### Notes

The authors declare the following competing financial interest(s): F.-G.K., T.S., and G.B. are co-authors and co-inventors of USA Patent No. 8,791,092 and European Patent Application 10 708 075.6. G.B. is a Director and a Co-Founder of Clear Therapeutics, Inc.

## ■ ACKNOWLEDGMENTS

We thank Dr. D. Teplow for the use of his CD spectrometer and microplate reader. The work was supported by a grant from the UCLA Jim Easton Consortium for Alzheimer's Drug Development and Biomarker Discovery (G.B.), a Liebig stipend (E.S.-G.), a predoctoral stipend from the Fonds der Chemischen Industrie (K.B.-R.) and the Deutsche Forschungsgemeinschaft (DFG) through the Cluster of Excellence RESOLV (EXC 1069) (E.S.-G., S. M., and K.B.-R) and the Collaborative Research Center SFB1093 (T.S., E.S.-G., S. M., and K.B.-R).

## ■ ABBREVIATIONS:

CD, circular dichroism; DTT, dithiothreitol; EM, electron microscopy; IAPP, islet amyloid polypeptide; MT, molecular tweezer; PB, phosphate buffer; REMD, replica-exchange molecular dynamics; T2D, type-2 diabetes; ThT, thioflavin T

## ■ REFERENCES

- (1) Tunis, S. L., and Minshall, M. E. (2008) Self-monitoring of blood glucose in type 2 diabetes: cost-effectiveness in the united states. *Am. J. Manag. Care* 14, 131–140.
- (2) American Diabetes Association (ADA) (2006) Diagnosis and classification of diabetes mellitus. *Diabetes Care* 29, S43–48.
- (3) Rossi, M. C., and Nicolucci, A. (2009) Liraglutide in type 2 diabetes: from pharmacological development to clinical practice. *Acta Biomed.* 80, 93–101.
- (4) Hogan, P., Dall, T., and Nikolov, P. (2003) Economic costs of diabetes in the US in 2002. *Diabetes Care* 26, 917–932.
- (5) Westermark, P., Wernstedt, C., O'Brien, T. D., Hayden, D. W., and Johnson, K. H. (1987) Islet amyloid in type 2 human diabetes mellitus and adult diabetic cats contains a novel putative polypeptide hormone. *Am. J. Pathol.* 127, 414–417.
- (6) Kapurniotu, A. (2001) Amyloidogenicity and cytotoxicity of islet amyloid polypeptide. *Biopolymers* 60, 438–459.
- (7) Rink, T. J., Beaumont, K., Koda, J., and Young, A. (1993) Structure and biology of amylin. *Trends Pharmacol. Sci.* 14, 113–118.
- (8) Knight, J. D., Hebda, J. A., and Miranker, A. D. (2006) Conserved and cooperative assembly of membrane-bound  $\alpha$ -helical states of islet amyloid polypeptide. *Biochemistry* 45, 9496–9508.
- (9) Williamson, J. A., Loria, J. P., and Miranker, A. D. (2009) Helix stabilization precedes aqueous and bilayer-catalyzed fiber formation in islet amyloid polypeptide. *J. Mol. Biol.* 393, 383–396.
- (10) Dupuis, N. F., Wu, C., Shea, J. E., and Bowers, M. T. (2009) Human islet amyloid polypeptide monomers form ordered  $\beta$ -hairpins: a possible direct amyloidogenic precursor. *J. Am. Chem. Soc.* 131, 18283–18292.
- (11) Westermark, P., Engstrom, U., Johnson, K. H., Westermark, G. T., and Betsholtz, C. (1990) Islet amyloid polypeptide: pinpointing amino acid residues linked to amyloid fibril formation. *Proc. Natl. Acad. Sci. U.S.A.* 87, 5036–5040.
- (12) Degaki, T. L., Lopes, D. H. J., and Sogayar, M. C. (2012) Cytotoxic mechanisms of islet amyloid polypeptide in the pathogenesis of type-2 diabetes mellitus (T2DM), in *Pre-fibrillar amyloidogenic protein assemblies—common cytotoxins underlying degenerative diseases* (Rahimi, A. F., and Bitan, G., Eds.), pp 217–256, Springer Science +Media B.V., Dordrecht, The Netherlands.
- (13) Luca, S., Yau, W. M., Leapman, R., and Tycko, R. (2007) Peptide conformation and supramolecular organization in amylin fibrils: constraints from solid-state NMR. *Biochemistry* 46, 13505–13522.
- (14) Reddy, A. S., Wang, L., Singh, S., Ling, Y. L., Buchanan, L., Zanni, M. T., Skinner, J. L., and de Pablo, J. J. (2010) Stable and metastable states of human amylin in solution. *Biophys. J.* 99, 2208–2216.
- (15) Miller, C., Zerze, G. H., and Mittal, J. (2013) Molecular simulations indicate marked differences in the structure of amylin

- mutants, correlated with known aggregation propensity. *J. Phys. Chem. B* 117, 16066–16075.
- (16) Murphy, R. D., Conlon, J., Mansoor, T., Luca, S., Vaiana, S. M., and Buchete, N. V. (2012) Conformational dynamics of human IAPP monomers. *Biophys. Chem.* 167, 1–7.
- (17) Dupuis, N. F., Wu, C., Shea, J. E., and Bowers, M. T. (2011) The amyloid formation mechanism in human IAPP: dimers have  $\beta$ -strand monomer-monomer interfaces. *J. Am. Chem. Soc.* 133, 7240–7243.
- (18) Laghaei, R., Mousseau, N., and Wei, G. (2011) Structure and thermodynamics of amylin dimer studied by Hamiltonian-temperature replica exchange molecular dynamics simulations. *J. Phys. Chem. B* 115, 3146–3154.
- (19) Qiao, Q., Bowman, G. R., and Huang, X. (2013) Dynamics of an intrinsically disordered protein reveal metastable conformations that potentially seed aggregation. *J. Am. Chem. Soc.* 135, 16092–16101.
- (20) Tomiyama, T., Kaneko, H., Kataoka, K., Asano, S., and Endo, N. (1997) Rifampicin inhibits the toxicity of pre-aggregated amyloid peptides by binding to peptide fibrils and preventing amyloid-cell interaction. *Biochem. J.* 322 (Pt 3), 859–865.
- (21) Lorenzo, A., Razzaboni, B., Weir, G. C., and Yankner, B. A. (1994) Pancreatic islet cell toxicity of amylin associated with type-2 diabetes mellitus. *Nature* 368, 756–760.
- (22) Aitken, J. F., Loomes, K. M., Konarkowska, B., and Cooper, G. J. (2003) Suppression by polycyclic compounds of the conversion of human amylin into insoluble amyloid. *Biochem. J.* 374, 779–784.
- (23) Harroun, T. A., Bradshaw, J. P., and Ashley, R. H. (2001) Inhibitors can arrest the membrane activity of human islet amyloid polypeptide independently of amyloid formation. *FEBS Lett.* 507, 200–204.
- (24) Levy, M., Porat, Y., Bacharach, E., Shalev, D. E., and Gazit, E. (2008) Phenolsulfonphthalein, but not phenolphthalein, inhibits amyloid fibril formation: implications for the modulation of amyloid self-assembly. *Biochemistry* 47, 5896–5904.
- (25) Hebda, J. A., Magzoub, M., and Miranker, A. D. (2014) Small molecule screening in context: lipid-catalyzed amyloid formation. *Protein Sci.* 23, 1341–1348.
- (26) Yan, L. M., Tatarek-Nossol, M., Velkova, A., Kazantzis, A., and Kapurniotu, A. (2006) Design of a mimic of nonamyloidogenic and bioactive human islet amyloid polypeptide (IAPP) as nanomolar affinity inhibitor of IAPP cytotoxic fibrillogenesis. *Proc. Natl. Acad. Sci. U.S.A.* 103, 2046–2051.
- (27) Meng, F., Abedini, A., Plesner, A., Middleton, C. T., Potter, K. J., Zanni, M. T., Verchere, C. B., and Raleigh, D. P. (2010) The sulfated triphenyl methane derivative acid fuchsin is a potent inhibitor of amyloid formation by human islet amyloid polypeptide and protects against the toxic effects of amyloid formation. *J. Mol. Biol.* 400, 555–566.
- (28) Scrocchi, L. A., Chen, Y., Waschuk, S., Wang, F., Cheung, S., Darabie, A. A., McLaurin, J., and Fraser, P. E. (2002) Design of peptide-based inhibitors of human islet amyloid polypeptide fibrillogenesis. *J. Mol. Biol.* 318, 697–706.
- (29) Saraogi, I., Hebda, J. A., Becerril, J., Estroff, L. A., Miranker, A. D., and Hamilton, A. D. (2009) Synthetic  $\alpha$ -Helix Mimetics as Agonists and Antagonists of Islet Amyloid Polypeptide Aggregation. *Angew. Chem., Int. Ed.* 49, 736–739.
- (30) Sinha, S., Lopes, D. H., Du, Z., Pang, E. S., Shanmugam, A., Lomakin, A., Talbiersky, P., Tennstaedt, A., McDaniel, K., Bakshi, R., Kuo, P. Y., Ehrmann, M., Benedek, G. B., Loo, J. A., Klärner, F. G., Schrader, T., Wang, C., and Bitan, G. (2011) Lysine-specific molecular tweezers are broad-spectrum inhibitors of assembly and toxicity of amyloid proteins. *J. Am. Chem. Soc.* 133, 16958–16969.
- (31) Acharya, S., Safaie, B. M., Wongkongkathep, P., Ivanova, M. I., Attar, A., Klärner, F. G., Schrader, T., Loo, J. A., Bitan, G., and Lapidus, L. J. (2014) Molecular basis for preventing  $\alpha$ -synuclein aggregation by a molecular tweezer. *J. Biol. Chem.* 289, 10727–10737.
- (32) Molt, O., Rubeling, D., and Schrader, T. (2003) A selective biomimetic tweezer for noradrenaline. *J. Am. Chem. Soc.* 125, 12086–12087.
- (33) Fokkens, M., Schrader, T., and Klärner, F. G. (2005) A molecular tweezer for lysine and arginine. *J. Am. Chem. Soc.* 127, 14415–14421.
- (34) Klärner, F. G., Kahlert, B., Nellesen, A., Zienau, J., Ochsenfeld, C., and Schrader, T. (2006) Molecular tweezer and clip in aqueous solution: Unexpected self-assembly, powerful host-guest complex formation, quantum chemical H-1 NMR shift calculation. *J. Am. Chem. Soc.* 128, 4831–4841.
- (35) Meng, F., Marek, P., Potter, K. J., Verchere, C. B., and Raleigh, D. P. (2008) Rifampicin does not prevent amyloid fibril formation by human islet amyloid polypeptide but does inhibit fibril thioflavin-T interactions: implications for mechanistic studies of  $\beta$ -cell death. *Biochemistry* 47, 6016–6024.
- (36) Prabhudesai, S., Sinha, S., Attar, A., Kotagiri, A., Fitzmaurice, A. G., Lakshmanan, R., Ivanova, M. I., Loo, J. A., Klärner, F. G., Schrader, T., Stahl, M., Bitan, G., and Bronstein, J. M. (2012) A novel “molecular tweezer” inhibitor of  $\alpha$ -synuclein neurotoxicity in vitro and in vivo. *Neurotherapeutics* 9, 464–476.
- (37) Yonemoto, I. T., Kroon, G. J., Dyson, H. J., Balch, W. E., and Kelly, J. W. (2008) Amylin proprotein processing generates progressively more amyloidogenic peptides that initially sample the helical state. *Biochemistry* 47, 9900–9910.
- (38) Tatarek-Nossol, M., Yan, L. M., Schmauder, A., Tenidis, K., Westermarck, G., and Kapurniotu, A. (2005) Inhibition of hIAPP amyloid-fibril formation and apoptotic cell death by a designed hIAPP amyloid-core-containing hexapeptide. *Chem. Biol.* 12, 797–809.
- (39) Zheng, X., Liu, D., Klärner, F.-G., Schrader, T., Bitan, G., and Bowers, M. T. (2015) Amyloid  $\beta$ -protein Assembly: The Effect of Molecular Tweezer CLR01 and CLR03. *J. Phys. Chem. B.* 119, 4831–4841.
- (40) Datki, Z., Juhasz, A., Galfi, M., Soos, K., Papp, R., Zadori, D., and Penke, B. (2003) Method for measuring neurotoxicity of aggregating polypeptides with the MTT assay on differentiated neuroblastoma cells. *Brain Res. Bull.* 62, 223–229.
- (41) Saafi, E. L., Konarkowska, B., Zhang, S., Kistler, J., and Cooper, G. J. (2001) Ultrastructural evidence that apoptosis is the mechanism by which human amylin evokes death in RINm5F pancreatic islet  $\beta$ -cells. *Cell Biol. Int.* 25, 339–350.
- (42) Duke, R. C., and Cohen, J. J. (1986) IL-2 addiction: withdrawal of growth factor activates a suicide program in dependent T cells. *Lymphokine Res.* 5, 289–299.
- (43) Bier, D., Rose, R., Bravo-Rodriguez, K., Bartel, M., Ramirez-Anguaita, J. M., Dutt, S., Wilch, C., Klärner, F. G., Sanchez-Garcia, E., Schrader, T., and Ottmann, C. (2013) Molecular tweezers modulate 14-3-3 protein-protein interactions. *Nat. Chem.* 5, 234–239.
- (44) Patil, S. M., Xu, S., Sheftic, S. R., and Alexandrescu, A. T. (2009) Dynamic  $\alpha$ -helix structure of micelle-bound human amylin. *J. Biol. Chem.* 284, 11982–11991.
- (45) Nanga, R. P., Brender, J. R., Vivekanandan, S., and Ramamoorthy, A. (2011) Structure and membrane orientation of IAPP in its natively amidated form at physiological pH in a membrane environment. *Biochim. Biophys. Acta* 1808, 2337–2342.
- (46) Talbiersky, P., Bastkowski, F., Klärner, F. G., and Schrader, T. (2008) Molecular clip and tweezer introduce new mechanisms of enzyme inhibition. *J. Am. Chem. Soc.* 130, 9824–9828.
- (47) Dutt, S., Wilch, C., Gersthagen, T., Wölper, C., Sowislok, A. A., Klärner, F.-G., and Schrader, T. (2013) Linker Effects on Amino Acid and Peptide Recognition by Molecular Tweezers. *Eur. J. Org. Chem.* 2013, 7705–7714.
- (48) Sparks, S., Liu, G., Robbins, K. J., and Lazo, N. D. (2012) Curcumin modulates the self-assembly of the islet amyloid polypeptide by disassembling  $\alpha$ -helix. *Biochem. Biophys. Res. Commun.* 422, 551–555.
- (49) Kumar, S., Brown, M. A., Nath, A., and Miranker, A. D. (2014) Folded small molecule manipulation of islet amyloid polypeptide. *Chem. Biol.* 21, 775–781.
- (50) Kumar, S., and Miranker, A. D. (2013) A foldamer approach to targeting membrane bound helical states of islet amyloid polypeptide. *Chem. Commun. (Cambridge, England)* 49, 4749–4751.

- (51) Liu, G., Prabhakar, A., Aucoin, D., Simon, M., Sparks, S., Robbins, K. J., Sheen, A., Petty, S. A., and Lazo, N. D. (2010) Mechanistic studies of peptide self-assembly: transient  $\alpha$ -helices to stable  $\beta$ -sheets. *J. Am. Chem. Soc.* 132, 18223–18232.
- (52) Zhou, R. (2007) Replica exchange molecular dynamics method for protein folding simulation. *Methods Mol. Biol.* 350, 205–223.
- (53) Butler, P. C., Chou, J., Carter, W. B., Wang, Y. N., Bu, B. H., Chang, D., Chang, J. K., and Rizza, R. A. (1990) Effects of meal ingestion on plasma amylin concentration in NIDDM and nondiabetic humans. *Diabetes* 39, 752–756.
- (54) Ogawa, A., Harris, V., McCorkle, S. K., Unger, R. H., and Luskey, K. L. (1990) Amylin secretion from the rat pancreas and its selective loss after streptozotocin treatment. *J. Clin. Invest.* 85, 973–976.
- (55) Lutz, T. A. (2010) The role of amylin in the control of energy homeostasis. *Am. J. Physiol. Regul. Integr. Comp. Physiol.* 298, R1475–1484.
- (56) Young, A. A., Rink, T. J., and Wang, M. W. (1993) Dose response characteristics for the hyperglycemic, hyperlactemic, hypotensive and hypocalcemic actions of amylin and calcitonin gene-related peptide-I (CGRP  $\alpha$ ) in the fasted, anaesthetized rat. *Life Sci.* 52, 1717–1726.
- (57) Ferreira, N., Pereira-Henriques, A., Attar, A., Klärner, F. G., Schrader, T., Bitan, G., Gales, L., Saraiva, M. J., and Almeida, M. R. (2014) Molecular tweezers targeting transthyretin amyloidosis. *Neurotherapeutics* 11, 450–461.
- (58) Attar, A., Chan, W. T., Klärner, F. G., Schrader, T., and Bitan, G. (2014) Safety and pharmacological characterization of the molecular tweezer CLR01 - a broad-spectrum inhibitor of amyloid proteins' toxicity. *BMC Pharmacol. Toxicol.* 15, 23.
- (59) Sinha, S., Du, Z., Maiti, P., Klärner, F. G., Schrader, T., Wang, C., and Bitan, G. (2012) Comparison of three amyloid assembly inhibitors: the sugar scyllo-inositol, the polyphenol epigallocatechin gallate, and the molecular tweezer CLR01. *ACS Chem. Neurosci.* 3, 451–458.
- (60) Attar, A., Ripoli, C., Riccardi, E., Maiti, P., Li Puma, D. D., Liu, T., Hayes, J., Jones, M. R., Lichti-Kaiser, K., Yang, F., Gale, G. D., Tseng, C. H., Tan, M., Xie, C. W., Straudinger, J. L., Klärner, F. G., Schrader, T., Frautschy, S. A., Grassi, C., and Bitan, G. (2012) Protection of primary neurons and mouse brain from Alzheimer's pathology by molecular tweezers. *Brain* 135, 3735–3748.
- (61) Sinha, S., Lopes, D. H., and Bitan, G. (2012) A key role for lysine residues in amyloid  $\beta$ -protein folding, assembly, and toxicity. *ACS Chem. Neurosci.* 3, 473–481.
- (62) Attar, A., and Bitan, G. (2014) Disrupting self-assembly and toxicity of amyloidogenic protein oligomers by “molecular tweezers” - from the test tube to animal models. *Curr. Pharm. Des.* 20, 2469–2483.
- (63) Jarrett, J. T., and Lansbury, P. T., Jr. (1993) Seeding “one-dimensional crystallization” of amyloid: A pathogenic mechanism in Alzheimer's disease and scrapie? *Cell* 73, 1055–1058.
- (64) Prusiner, S. B. (2012) Cell biology. A unifying role for prions in neurodegenerative diseases. *Science* 336, 1511–1513.
- (65) Lopes, D. H., Sinha, S., Rosensweig, C., and Bitan, G. (2012) Application of photochemical cross-linking to the study of oligomerization of amyloidogenic proteins. *Methods Mol. Biol.* 849, 11–21.
- (66) Rahimi, F., Murakami, K., Summers, J. L., Chen, C. H. B., and Bitan, G. (2009) RNA aptamers generated against oligomeric A $\beta$ 40 recognize common amyloid aptatopes with low specificity but high sensitivity. *PLoS One* 4, e7694.
- (67) Maiti, P., Piacentini, R., Ripoli, C., Grassi, C., and Bitan, G. (2010) Surprising toxicity and assembly behaviour of amyloid  $\beta$ -protein oxidized to sulfone. *Biochem. J.* 433, 323–332.
- (68) Corsaro, A., Thellung, S., Villa, V., Principe, D. R., Paludi, D., Arena, S., Millo, E., Schettini, D., Damonte, G., Aceto, A., Schettini, G., and Florio, T. (2003) Prion protein fragment 106–126 induces a p38 MAP kinase-dependent apoptosis in SH-SY5Y neuroblastoma cells independently from the amyloid fibril formation. *Ann. N.Y. Acad. Sci.* 1010, 610–622.
- (69) Mackerell, A. D., Jr., Feig, M., and Brooks, C. L., 3rd (2004) Extending the treatment of backbone energetics in protein force fields: limitations of gas-phase quantum mechanics in reproducing protein conformational distributions in molecular dynamics simulations. *J. Comput. Chem.* 25, 1400–1415.
- (70) Zoete, V., Cuendet, M. A., Grosdidier, A., and Michielin, O. (2011) SwissParam: a fast force field generation tool for small organic molecules. *J. Comput. Chem.* 32, 2359–2368.
- (71) Dutt, S., Wilch, C., Gersthagen, T., Talbiersky, P., Bravo-Rodriguez, K., Hanni, M., Sanchez-Garcia, E., Ochsenfeld, C., Klärner, F. G., and Schrader, T. (2013) Molecular tweezers with varying anions: a comparative study. *J. Org. Chem.* 78, 6721–6734.
- (72) Hess, B., Kutzner, C., van der Spoel, D., and Lindahl, E. (2008) GROMACS 4: Algorithms for highly efficient, load-balanced, and scalable molecular simulation. *J. Chem. Theory Comput* 4, 435–447.
- (73) Jorgensen, W. L., Chandrasekhar, J., Madura, J. D., Impey, R. W., and Klein, M. L. (1983) Comparison of Simple Potential Functions for Simulating Liquid Water. *J. Chem. Phys.* 79, 926–935.
- (74) Tironi, I. G., Sperb, R., Smith, P. E., and Vangunsteren, W. F. (1995) A Generalized Reaction Field Method for Molecular-Dynamics Simulations. *J. Chem. Phys.* 102, 5451–5459.
- (75) Hess, B., Bekker, H., Berendsen, H. J. C., and Fraaije, J. G. E. M. (1997) LINCS: A linear constraint solver for molecular simulations. *J. Comput. Chem.* 18, 1463–1472.
- (76) Darden, T., York, D., and Pedersen, L. (1993) Particle mesh Ewald - an  $N \log(N)$  method for Ewald sums in large systems. *J. Chem. Phys.* 98, 10089–10092.
- (77) Essmann, U., Perera, L., Berkowitz, M. L., Darden, T., Lee, H., and Pedersen, L. G. (1995) A smooth particle mesh Ewald method. *J. Chem. Phys.* 103, 8577–8593.
- (78) Patriksson, A., and van der Spoel, D. (2008) A temperature predictor for parallel tempering simulations. *Phys. Chem. Chem. Phys.* 10, 2073–2077.
- (79) Okabe, T., Kawata, M., Okamoto, Y., and Mikami, M. (2001) Replica-exchange Monte Carlo method for the isobaric-isothermal ensemble. *Chem. Phys. Lett.* 335, 435–439.
- (80) Hukushima, K., and Nemoto, K. (1996) Exchange Monte Carlo method and application to spin glass simulations. *J. Phys. Soc. Jpn.* 65, 1604–1608.
- (81) Daura, X., Gademann, K., Jaun, B., Seebach, D., van Gunsteren, W. F., and Mark, A. E. (1999) Peptide folding: When simulation meets experiment. *Angew. Chem., Int. Ed.* 38, 236–240.

## NOTE ADDED AFTER ASAP PUBLICATION

This paper was originally published ASAP on April 16, 2015. Heinz Bandmann was added to the author list, and the paper was reposted on April 20, 2015.